

*Journal of Hydrology*, Vol. 389, No. 1-2, 2010, pp. 146-167

---

1     **Prediction of Rainfall Time Series Using Modular Artificial Neural Networks Coupled**  
2                                    **with Data Preprocessing Techniques**

3                                    C. L. Wu<sup>1,2</sup>, K. W. Chau<sup>1,\*</sup>, and C. Fan<sup>3</sup>

4                                    <sup>1</sup>Dept. of Civil and Structural Engineering, Hong Kong Polytechnic University,

5                                    Hung Hom, Kowloon, Hong Kong, People's Republic of China

6  
7                                    <sup>2</sup>Changjiang Institute of Survey, Planning, Design and Research,

8                                    Changjiang Water Resources Commission,

9                                    430010, Wuhan, HuBei, People's Republic of China

10  
11                                   <sup>3</sup>Department of Civil Engineering, Ryerson University,

12                                   350 Victoria Street, Toronto, Ontario, Canada, M5B 2K3

13  
14                                    \*Email: [cekwchau@polyu.edu.hk](mailto:cekwchau@polyu.edu.hk)

15  
16     **ABSTRACT**

17     This study is an attempt to seek a relatively optimal data-driven model for rainfall forecasting from three aspects:  
18     model inputs, modeling methods, and data preprocessing techniques. Four rain data records from different  
19     regions, namely two monthly and two daily series, are examined. A comparison of seven input techniques,  
20     either linear or nonlinear, indicates that linear correlation analysis (LCA) is capable of identifying model inputs  
21     reasonably. A proposed model, modular artificial neural network (MANN), is compared with three benchmark  
22     models, viz. artificial neural network (ANN), K-nearest-neighbors (K-NN), and linear regression (LR).  
23     Prediction is performed in the context of two modes including normal mode (viz., without data preprocessing)  
24     and data preprocessing mode. Results from the normal mode indicate that MANN performs the best among all  
25     four models, but the advantage of MANN over ANN is not significant in monthly rainfall series forecasting.  
26     Under the data preprocessing mode, each of LR, K-NN and ANN is respectively coupled with three data

27 preprocessing techniques including moving average (MA), principal component analysis (PCA), and singular  
28 spectrum analysis (SSA). Results indicate that the improvement of model performance generated by SSA is  
29 considerable whereas those of MA or PCA are slight. Moreover, when MANN is coupled with SSA, results  
30 show that advantages of MANN over other models are quite noticeable, particularly for daily rainfall  
31 forecasting. Therefore, the proposed optimal rainfall forecasting model can be derived from MANN coupled  
32 with SSA.

### 33 **KEYWORDS**

34 Rainfall prediction, Modular artificial neural network, Moving Average, Principal component analysis, Singular  
35 spectral analysis, Fuzzy C-Means clustering, K-nearest-neighbors

36

## 37 **1. Introduction**

38 Accurate and timely rainfall forecasting is crucial for reservoir operation and flooding  
39 prevention because it can provide an extension of lead-time of the flow forecasting, larger  
40 than the response time of the watershed, in particular for small and medium-sized  
41 mountainous basins.

42 Many studies have been conducted for the quantitative precipitation forecasting using  
43 diverse techniques including numerical weather prediction models and remote sensing  
44 observations (Yates et al., 2000; Ganguly and Bras, 2003; Sheng, et al., 2006; Doomedede et al.,  
45 2008), statistical models (Chu and He, 1995; Chan and Shi, 1999; DelSole and Shukla, 2002;  
46 Munot, 2007; Li and Zeng, 2008; Nayagam et al., 2008), chaos theory-based approach  
47 (Jayawardena and Lai, 1994), K-nearest-neighbor (K-NN) method (Toth et al, 2000), and soft  
48 computing methods including artificial neural network (ANN), support vectors regression  
49 (SVR) and fuzzy inference system (Venkatesan et al., 1997; Silverman and Dracup, 2000;

50 Toth et al., 2000; Pongracz et al., 2001; Sivapragasam et al., 2001; Brath et al., 2002; Lin and  
51 Chen, 2005; Chattopadhyay and Chattopadhyay, 2007; Guhathakurta, 2008; Lin et al., 2009).  
52 Venkatesan et al. (1997) employed ANN to predict all India summer monsoon rainfall with  
53 different meteorological parameters as model inputs. Toth et al. (2000) applied three data-  
54 driven models, auto-regressive moving average, ANN and K-NN, to short-term rainfall  
55 predictions. Results showed that ANN performed the best in terms of the accuracy of runoff  
56 forecasting when the predicted rainfalls by the three models were used as inputs of a rainfall-  
57 runoff model. Pongracz et al. (2001) applied fuzzy inference to monthly rainfall prediction.  
58 Chattopadhyay and Chattopadhyay (2007) constructed an ANN model to predict monsoon  
59 rainfall in India depending on the rainfall series alone.

60         Recently, the concept of coupling different models has attracted more attention in  
61 hydrologic forecasting. They can be broadly categorized into ensemble models and modular  
62 (or hybrid) models. The basic idea behind ensemble models is to build several different or  
63 similar models for the same process and to integrate them together (Shamseldin et al., 1997;  
64 Shamseldin and O'Connor, 1999; Xiong et al., 2001; Abrahart and See, 2002; Kim et al.,  
65 2006). For example, Xiong et al. (2001) used a Takagi-Sugeno-Kang fuzzy technique to  
66 couple several conceptual rainfall-runoff models. Coulibaly et al. (2005) employed an  
67 improved weighted-average method to coalesce forecasted daily reservoir inflows from K-  
68 NN, conceptual model and ANN. Kim et al. (2006) investigated five ensemble methods for  
69 improving stream flow prediction.

70         Physical processes in rainfall and/or runoff are generally composed of a number of  
71 sub-processes. Their accurate modeling by building of a single global model is sometimes not  
72 possible (Solomatine and Ostfeld, 2008). Modular models were therefore proposed where

73 sub-processes were first of all identified and then separate models (also called local or expert  
74 model) were established for each of them (Solomatine and Ostfeld, 2008). Different modular  
75 models were proposed depending on the soft or hard splitting of training data. Soft splitting  
76 means the dataset can be overlapped and the overall forecasting output is the weighted-  
77 average of each local model (Zhang and Govindaraju, 2000; Shrestha and Solomatine, 2006;  
78 Wu et al., 2008). Zhang and Govindaraju (2000) examined the performance of modular  
79 networks in predicting monthly discharges based on the Bayesian concept. Wu et al. (2008)  
80 employed a distributed SVR for daily river stage prediction. On the contrary, there is no  
81 overlap of data in the hard splitting and the final forecasting output is explicitly from only  
82 one of local models (See and Openshaw, 2000; Hu et al., 2001; Solomatine and Xue, 2004;  
83 Sivapragasam and Liong, 2005; Jain and Srinivasulu, 2006; Wang et al., 2006; Corzo and  
84 Solomatine, 2007; Lin and Wu, 2009). Hu et al. (2001) developed a range-dependent network  
85 which employs a number of multilayer perceptron neural networks to model the river flow in  
86 different flow bands of magnitude (e.g. high, medium and low). Their results indicated that  
87 the range-dependent network performed better than the conventional global ANN.  
88 Solomatine and Xue (2004) used M5 model trees and neural networks in a flood-forecasting  
89 problem. Sivapragasam and Liong (2005) divided the flow range into three regions, and  
90 employed different SVR models to predict daily flows in high, medium and low regions.  
91 Wang et al. (2006) used a crisp modular ANN to make soft or crisp predictions for validation  
92 data where each local network was trained using the subsets achieved by either a threshold  
93 discharge value or a clustering of input spaces. Lin and Wu (2009) proposed a hybrid ANN  
94 model for event-based hourly rainfall prediction where self-organizing map networks are

95 used for data cluster analysis and multilayer conception networks are employed to serve each  
96 cluster to construct mapping between input and output.

97         A hydrological time series can be actually regarded as an integration of stochastic (or  
98 random) and deterministic components (Salas et al., 1985). Once the stochastic (noise)  
99 component is appropriately eliminated, the deterministic component can then be easily  
100 modeled. For the purpose of cleaning hydrological series, many data preprocessing  
101 techniques, including Principal component analysis (PCA), wavelet analysis (WA), and  
102 singular spectrum analysis (SSA), have been employed in hydrology field by researchers  
103 (Sivapragasam et al., 2001; Marques et al., 2006; Hu et al., 2007; Partal and Kişi, 2007;  
104 Sivapragasam et al., 2007; Wu et al., 2009). Hu et al. (2007) employed PCA as an input data  
105 preprocessing tool to improve the prediction accuracy of the rainfall-runoff neural network  
106 models. The use of WA to improve rainfall forecasting was conducted by Partal and Kişi  
107 (2007). Their results indicated that WA was promising. SSA has also been recognized as an  
108 efficient preprocessing algorithm to avoid the effect of discontinuous or intermittent signals,  
109 coupled with neural networks (or similar approaches) for time series forecasting (Lisi et al.,  
110 1995; Sivapragasam et al., 2001; Baratta et al., 2003). For example, Lisi et al. (1995) applied  
111 SSA to extract the significant components in their study on southern oscillation index time  
112 series and used ANN for prediction. They reconstructed the original series by summing up  
113 the first “p” significant components. Sivapragasam et al. (2001) proposed a hybrid model of  
114 support vector machine (SVM) and SSA for rainfall and runoff predictions. The hybrid  
115 model resulted in a considerable improvement in the model performance in comparison with  
116 the original SVM model. A comparison between WA and SSA in Wu et al. (2009) indicated  
117 that SSA performed better than WA. In addition, moving average (MA) is used for data

118 preprocessing to improve the performance of ANN by de Vos and Rientjes (2005). They  
119 argued that one of reasons on lagged predictions of ANN was due to the use of previous  
120 observed data as ANN inputs and suggested that an effective solution was to obtain new  
121 model inputs by MA over the original data series.

122 In this paper, one of the main purposes is to develop a modular ANN (MANN)  
123 coupled with appropriate data-preprocessing techniques to improve the accuracy of rainfall  
124 forecasting. MANN consists of three local models which are associated with three subsets  
125 clustered by the fuzzy C-means (FCM) clustering method. To evaluate MANN, LR, K-NN  
126 and ANN are employed for comparison. ANN is first used to choose the best model inputs by  
127 seven candidate model inputs techniques. Once all forecasting models are established, three  
128 data-preprocessing methods (i.e., MA, PCA, and SSA) can be examined. To ensure wider  
129 application of the conclusions, four cases consisting of two monthly rainfall series and two  
130 daily rainfall series from India and China, are investigated. The remaining part is structured  
131 as follows. Methodology is detailed in Section 2 where case studies are first described, and  
132 then data-preprocessing techniques and forecasting models are introduced. Section 3 presents  
133 modeling methods and their applications to four rainfall series. The optimal model input  
134 method and the best data preprocessing can be identified. In Section 4, principal results are  
135 shown along with relevant discussions. The last section presents main conclusions.

## 136 **2. Methodology**

### 137 **2.1 Study Area and Data**

138 Two daily mean rainfall series from Daning and Zhenshui river basins of China, and  
139 two monthly mean rainfall series from India and Zhongxian of China, are analyzed.

140 The Daning River, a first-order tributary of the Yangtze River, is located at the  
141 northeastern side of Chongqing city. The daily rainfall data from Jan. 1, 1988 to Dec. 31,  
142 2007 were measured at six raingauges located at the upstream of the study basin (Figure 1).  
143 The upstream part is controlled by Wuxi hydrology station, with a drainage area of around 2  
144 000 km<sup>2</sup>. The mean areal rainfall series is calculated by the Thiessen polygon method  
145 (hereafter the averaged rainfall series is referred to as Wuxi).

146 The Zhenshui basin is located at the northern side of Guangdong Province and  
147 adjoined by Hunan Province and Jianxi Province. The basin belongs to a second-order  
148 tributary of the Pearl River and has an area of 7,554 km<sup>2</sup>. The daily rainfall time series of  
149 Zhenwan raingauge was collected between January 1, 1989 and December 31, 1998  
150 (hereafter the averaged rainfall series is referred to as Zhenwan).

151 The all Indian average monthly rainfall is estimated from area-weighted observations  
152 at 306 land stations uniformly distributed over India. The data, with period spanning from  
153 January 1871 to December 2007, are available at the website <http://www.tropmet.res.in> run  
154 by the Indian Institute of Tropical Meteorology.

155 The other monthly rainfall series is from Zhongxian raingauge which is located at  
156 Chongqing city, China. The catchment containing this raingauge belongs to a first-order  
157 tributary of the Yangtze River. The monthly rainfall data were collected from January 1956  
158 to December 2007.

159 Figure 2 shows hyetographs of four rainfall series. A linear fit to each hyetograph is  
160 denoted by the dashed line. All series appear stationary at least in a weak sense since these  
161 linear fits are close to horizontal.

162 In this study, each of data series is partitioned into three parts as training set, cross-  
163 validation set and testing set. The training set serves the model training and the testing set is  
164 used to evaluate the performances of models. The cross-validation set has dual functions: one  
165 is to implement an early stopping approach in order to avoid overfitting of the training data  
166 and another is to select some best predictions from a number of ANN's runs. In the present  
167 study, 10 best predictions are selected from a total of 20 ANN's runs. The same data partition  
168 is adopted for each series: the first half of the entire data as training set and the first half of  
169 the remaining data as cross-validation set and the other half as testing set.

170 Table 1 presents pertinent information about watersheds and some descriptive  
171 statistics of the original data and three data subsets, including mean ( $\mu$ ), standard deviation  
172 ( $S_x$ ), coefficient of variation ( $C_v$ ), skewness coefficient ( $C_s$ ), minimum ( $X_{\min}$ ), and maximum  
173 ( $X_{\max}$ ). As shown in Table 1, the training set cannot fully include the cross-validation or  
174 testing data. Owing to the weak extrapolation ability of ANN, all data are scaled to the  
175 interval [-0.9, 0.9] instead of [-1, 1] whilst hyperbolic tangent sigmoid functions are  
176 employed as transfer functions in hidden and output layers.

## 177 **2.2 Data preprocessing techniques**

### 178 **(1) MA**

179 MA smoothes data by replacing each data point with the average of the  $k$   
180 neighboring data points, where  $k$  may be termed the length of memory window. The method  
181 is based on the idea that any large irregular component at any point in time will exert a  
182 smaller effect if we average the point with its immediate neighbors (Newbold et al., 2003).  
183 The equally weighted MA is the most commonly-used, in which each value of the data  
184 carries the same weight in the smoothing process. There are three types of moving modes



185 including centering, backward and forward. In a forecasting scenario, only the backward  
186 mode is used since the other two modes may necessitate future observed values. For a time  
187 series  $\{x_1, x_2, \dots, x_N\}$ , when the backward moving mode is adopted (Lee et al., 2000), the  
188  $k$ -term unweighted moving average  $y_t^*$  is written as

$$189 \quad y_t^* = \left( \sum_{i=0}^{k-1} y_{t-i} \right) / k \quad (1)$$

190 where  $t = k, \dots, N$ . The choice of the window length  $k$  is by a trial and error procedure with  
191 a minimization of the loss of the objective function.

## 192 (2) PCA

193 PCA was first introduced by Pearson (1901) and developed independently by  
194 Hotelling (1933), and has now well entrenched as an important technique in data analysis.  
195 The central idea is to reduce the dimensionality of a data set consisting of a large number of  
196 interrelated variables, while retaining as much as possible of the variation present in the data  
197 set. The PCA approach uses all of the original variables to obtain a smaller set of principal  
198 components (PCs) which can be used to approximate the original variables. PCs are  
199 uncorrelated and are ordered so that the first few retain most of the variation present in the  
200 original set.

201 Consider a data matrix  $\mathbf{X}$  which has  $n$  rows (observations) and  $p$  column (variables).

202 Let the covariance matrix of  $\mathbf{X}$  be  $\Sigma$ , where  $\Sigma = \text{cov}(\mathbf{X}) = E(\mathbf{X}^T \mathbf{X})$ . The linear transformed  
203 orthogonal matrix  $\mathbf{Z}$  is presented as

$$204 \quad \mathbf{Z} = \mathbf{X}\mathbf{A} \quad (2)$$

205 where  $\mathbf{Z}$  is the PCs with elements  $(i, j)$  of  $i$ th observation and  $j$ th principal component;  $\mathbf{A}$   
206 is a  $(p \times p)$  matrix with eigenvector elements of the covariance of  $\mathbf{X}$ , and having  
207  $\mathbf{A}^T \mathbf{A} = \mathbf{A} \mathbf{A}^T = \mathbf{I}$ .

208 Because matrix  $\mathbf{X}^T \mathbf{X}$  is real and symmetric, it can be expressed as  $\mathbf{X}^T \mathbf{X} = \mathbf{A} \mathbf{\Lambda} \mathbf{A}^T$   
209 where  $\mathbf{\Lambda}$  is a diagonal matrix whose nonnegative entries are the eigenvalues  $(\lambda_i, i = 1, \dots, p)$   
210 of  $\mathbf{X}^T \mathbf{X}$ . The total variance of the data matrix  $\mathbf{X}$  is represented as

$$211 \quad \text{trace}(\mathbf{\Sigma}) = \text{trace}(\mathbf{A} \mathbf{\Lambda} \mathbf{A}^T) = \text{trace}(\mathbf{\Lambda}) = \sum_{i=1}^p \lambda_i \quad (3)$$

212 On the other hand, the covariance matrix of principal components  $\mathbf{Z}$  is expressed as

$$213 \quad \text{cov}(\mathbf{Z}) = E(\mathbf{Z}^T \mathbf{Z}) = E(\mathbf{A}^T \mathbf{X}^T \mathbf{X} \mathbf{A}) = \mathbf{\Lambda} \quad (4)$$

$$214 \quad \text{trace}(\mathbf{Z}) = \text{trace}(\mathbf{\Lambda}) = \sum_{i=1}^p \lambda_i \quad (5)$$

215 Therefore, the total variance of the data matrix  $\mathbf{X}$  is identical to the total variance after PCA  
216 transformation  $\mathbf{Z}$ .

217 The solution of PCA, using singular value decomposition (SVD) or determinants of  
218 the covariance matrix of  $\mathbf{X}$ , can provide the eigenvectors  $\mathbf{A}$  with their  
219 eigenvalues,  $\lambda_i, i = 1, \dots, p$ , representing the variance of each component after PCA  
220 transformation. If the eigenvalues are ordered by  $\lambda_1 \geq \lambda_2 \geq \lambda_3 \geq \dots \geq \lambda_p \geq 0$ , the first few PCs  
221 can capture most of the variance of the original data while the remaining PCs mainly  
222 represent the noise in the data. The percentage of total variance explained by the first  $m$ th  
223 PCs is

$$224 \quad V = \sum_{i=1}^m \lambda_i / \sum_{i=1}^p \lambda_i \cdot 100\% \quad (6)$$

225 The higher is the selection of the total data variance,  $V$ , the better the properties of the data  
226 matrix are preserved. For the sake of the reduction of dimensionality, a small number of PCs  
227 are selected, though most of the data variance in selected components still remain. If the  
228 transformation is to prevent the collinearity of regression variables, the selected component  
229 number  $m$  in Eq. (6) can be set for a higher total variance, such as  $V = 95\% \square 99\%$  (Hsu et  
230 al., 2002).

231 The original data matrix  $\mathbf{A}$  can be reconstructed by a reverse operation of Eq. (2) as

$$232 \quad \mathbf{X} = \mathbf{Z}\mathbf{A}^T \quad (7)$$

233 By choosing suitable  $m$  ( $\leq p$ ) PCs from  $\mathbf{Z}$  and accompanying  $m$  eigenvectors from  $\mathbf{A}$ , the  
234 original data can be filtered.

### 235 (3) SSA

236 According to Golyandina et al. (2001), the basic SSA consists of two stages:  
237 decomposition and reconstruction. The decomposition stage involves two steps: embedding  
238 and SVD; the reconstruction stage also comprises two steps: grouping and diagonal  
239 averaging. Consider a real-valued time series  $F = \{x_1, x_2, \dots, x_N\}$  of length  $N(> 2)$ . Assume  
240 that the series is a nonzero series, viz. there exists at least one  $i$  such that  $x_i \neq 0$ . Four steps  
241 are briefly presented as follows.

#### 242 *1st step: embedding*

243 The embedding procedure maps the original time series to a sequence of multi-  
244 dimensional lagged vectors. Let  $L$  be an integer (window length),  $1 < L < N$ , and  $\tau$  be the  
245 delayed time at a multiple of the sampling period. The embedding procedure forms  
246  $n = N - (L - 1)\tau$  lagged vectors  $\mathbf{x}_i = \{x_i, x_{i+\tau}, x_{i+2\tau}, \dots, x_{i+(L-1)\tau}\}^T$ , where  $\mathbf{x}_i \in \mathbf{R}^L$ , and

247  $i = 1, 2, \dots, n$ . The ‘trajectory matrix’ of the time series is denoted by  $\mathbf{X} = [\mathbf{X}_1 \ \dots \ \mathbf{X}_i \ \dots \ \mathbf{X}_n]$   
 248 having lagged vectors as its columns. In other words, the trajectory matrix is

$$249 \quad \mathbf{X} = \begin{pmatrix} x_1 & x_2 & x_3 & \dots & x_n \\ x_{1+\tau} & x_{2+\tau} & x_{3+\tau} & \dots & x_{n+\tau} \\ x_{1+2\tau} & x_{2+2\tau} & x_{3+2\tau} & \dots & x_{n+2\tau} \\ \vdots & \vdots & \vdots & \vdots & \vdots \\ x_{1+(L-1)\tau} & x_{2+(L-1)\tau} & x_{3+(L-1)\tau} & \dots & x_N \end{pmatrix} \quad (8)$$

250 If  $\tau = 1$ , the matrix  $\mathbf{X}$  is called Hankel matrix since it has equal elements on the  
 251 ‘diagonals’ where the sum of subscripts of row and column is equal to constant. If  $\tau > 1$ , the  
 252 equal elements in  $\mathbf{X}$  are not definitely in the ‘diagonals’.

253 **2nd step: SVD**

254 Let  $\mathbf{S} = \mathbf{X}\mathbf{X}^T$ ,  $\lambda_1, \lambda_2, \dots, \lambda_L$  denote the eigenvalues of  $\mathbf{S}$  taken in the decreasing order  
 255 of magnitude ( $\lambda_1 \geq \lambda_2 \geq \lambda_3 \geq \dots \geq \lambda_L \geq 0$ ) and  $\mathbf{u}_1, \mathbf{u}_2, \dots, \mathbf{u}_L$  denote the orthonormal system of  
 256 the eigenvectors of the matrix  $\mathbf{S}$  corresponding to these eigenvalues. If we denote  
 257  $\mathbf{v}_i = \mathbf{X}_i^T \mathbf{u}_i / \sqrt{\lambda_i}$  ( $i = 1, \dots, L$ ) (equivalent to the  $i$ th eigenvector of  $\mathbf{X}^T \mathbf{X}$ ), then the SVD of the  
 258 trajectory matrix  $\mathbf{X}$  can be written as

$$259 \quad \mathbf{X} = \mathbf{X}_1 + \dots + \mathbf{X}_L \quad (9)$$

260 where  $\mathbf{X}_i = \sqrt{\lambda_i} \mathbf{u}_i \mathbf{v}_i^T$ . The matrices  $\mathbf{X}_i$  have rank 1; therefore they are elementary matrices.  
 261 The collection  $(\lambda_i, \mathbf{u}_i, \mathbf{v}_i)$  is called the  $i$ th eigentriple of the SVD. Note that  $\mathbf{u}_i$  and  $\mathbf{v}_i$  are  
 262 also the  $i$ th left and right singular vectors of  $\mathbf{X}$ , respectively.

263 **3rd step: grouping**

264 The purpose of this step is to identify appropriately the trend component, oscillatory  
 265 components with different periods, and structureless noises by grouping components. This

266 step can be skipped if one does not want to precisely extract hidden information by  
267 regrouping and filtering of components.

268 The grouping procedure partitions the set of indices  $\{1, \dots, L\}$  into  $m$  disjoint subsets  
269  $I_1, \dots, I_m$ , so that the elementary matrix in Eq. (9) is regrouped into  $m$  groups. Let  
270  $I = \{i_1, \dots, i_p\}$ . Then the resultant matrix  $\mathbf{X}_I$  corresponding to the group  $I$  is defined as  
271  $\mathbf{X}_I = \mathbf{X}_{i_1} + \dots + \mathbf{X}_{i_p}$ . These matrices are computed for  $I_1, \dots, I_m$ . By substituting into the  
272 expansion (9), one obtains the new expansion

$$273 \quad \mathbf{X} = \mathbf{X}_{I_1} + \dots + \mathbf{X}_{I_m} \quad (10)$$

274 The procedure of choosing the sets  $I_1, \dots, I_m$  is called the eigentriple grouping.

#### 275 ***4th step: Diagonal averaging***

276 The last step in the basic SSA is the transformation of each resultant matrix of the  
277 grouped decomposition (10) into a new series of length  $N$ . The diagonal averaging is to find  
278 equal elements in the resultant matrix and then to generate a new element by averaging over  
279 them. The new element has the same position (or index) as the corresponding elements in the  
280 original series. As mentioned in the step 1, the concept of ‘diagonal’ is not true for  $\tau > 1$ .  
281 Regardless of the value of  $\tau$  being larger than or equal to 1, the principle of reconstruction is  
282 the same. For  $\tau = 1$ , the diagonal averaging can be carried out by the formula recommended  
283 by Golyandina et al. (2001). Let  $\mathbf{Y}$  be a  $(L \times n)$  matrix with elements  $y_{ij}$ ,  $1 \leq i \leq L$ ,  $1 \leq j \leq n$ .  
284 Let  $L^* = \min(L, n)$ ,  $n^* = \max(L, n)$  and  $N = n + (L-1)\tau$ . Let  $y_{ij}^* = y_{ij}$  if  $L < n$  and  $y_{ij}^* = y_{ji}$   
285 otherwise. Diagonal averaging transfers matrix  $\mathbf{Y}$  to a series  $\{y_1, y_2, \dots, y_N\}$  by the following  
286 equation

$$y_k = \begin{cases} \frac{1}{k} \sum_{m=1}^k y_{m,k-m+1}^* & \text{for } 1 \leq k < L^* \\ \frac{1}{L^*} \sum_{m=1}^{L^*} y_{m,k-m+1}^* & \text{for } L^* \leq k \leq K^* \\ \frac{1}{N-k+1} \sum_{m=k-K^*+1}^{N-K^*+1} y_{m,k-m+1}^* & \text{for } L^* < k \leq N \end{cases} \quad (11)$$

Eq. (11) corresponds to the averaging of the matrix elements over the ‘diagonals’  $i + j = k + 1$ .

The diagonal averaging, applied to a resultant matrix  $\mathbf{X}_{I_k}$ , produces a  $N$ –length series  $F_k$ ,

and thus the original series  $F$  is decomposed into the sum of  $m$  series:

$$F = F_1 + \dots + F_m \quad (12)$$

As mentioned above, these reconstructed components (RCs) can be associated with the trend, oscillations or noise of the original time series with proper choices of  $L$  and the sets of  $I_1, \dots, I_m$ . Certainly, if the third step (namely, grouping) is skipped,  $F$  can be decomposed into  $L$ RCs.

### 2.3 Forecasting models

This section describes four candidate forecasting models. They are LR, K-NN, ANN and MANN. They are usually called data-driven models because they capture the mapping between input (e.g. antecedent rainfall) and output variables (forecasted rainfall) without directly considering the physical laws that underlie the mechanism of rainfall (or precipitation). These models are purely based on the information retrieved from the collected rainfall data.

#### (1) Construction of input/output pairs

304 Let  $\{x_1, x_2, \dots, x_N\}$  stand for a rainfall time series. It can be reconstructed into a series  
305 of delay vectors as  $\mathbf{X}_t = \{x_t, x_{t+\tau}, x_{t+2\tau}, \dots, x_{t+(m-1)\tau}\}$ , where  $\mathbf{X}_t \in \mathbb{R}^m$ ,  $\tau$  is the delay time as a  
306 multiple of the sampling period and  $m$  is the embedded dimension. Suppose that the rainfall  
307  $x_{t+T+(m-1)\tau}$  at  $T$ -step lead is related to the vector  $\mathbf{X}_t$ , the available historical data may be  
308 summarized into a set of pairs as  $\{\mathbf{X}_t, x_{t+T+(m-1)\tau} : t = 1, \dots, n\}$ , where  $n$  stands for the number of  
309 pairs, and  $n = N - (m-1)\tau$ .

310 The functional relationship between the input vector  $\mathbf{X}_t$  at time  $t$  and the predicted  
311 output  $x_{t+T+(m-1)\tau}^F$  at time  $t+T$  can be written as follows:

$$312 \quad x_{t+T+(m-1)\tau}^F = f(\mathbf{X}_t) + e_t \quad (13)$$

313 where  $e_t$  is a typical noise term,  $x_{t+T+(m-1)\tau}^F$  is the prediction of  $x_{t+T+(m-1)\tau}$ , and  $f(\bullet)$  is the  
314 mapping function. The difference of various data-driven forecasting models used in the  
315 current study relies on the way of approximating  $f(\bullet)$  once model inputs are attained with  
316 the appropriate selection of  $(\tau, m)$ .

## 317 (2) LR

318 The linear regression model herein is actually called stepwise linear regression (SLR)  
319 model because the forward stepwise regression is used to determine optimal input variables.  
320 The basic idea of SLR is to start with a function that contains the single best input variable  
321 and to subsequently add potential input variables to the function one at a time in an attempt to  
322 improve the model performance. The order of addition is determined by using the partial  
323  $F$ -test values to select which variable should enter next. The high partial  $F$ -value is  
324 compared to a (selected or default)  $F$ -to-enter value. After a variable has been added, the

325 function is examined to see if any variable should be deleted. Interested readers are referred  
 326 to Draper and Smith (1998) and McCuen (2005) for more details.

327 **(3) K-NN**

328 The prediction of  $x_{t+T+(m-1)\tau}$  by the K-NN method is formulated as:

$$329 \quad x_{t+T+(m-1)\tau}^F = \frac{1}{K} \sum_{t \in S(\mathbf{X}, n)} x_{t+T+(m-1)\tau} \quad (14)$$

330 where  $S(\mathbf{X}, n)$  denotes the set of indices  $t$  of the  $K$  nearest neighbors to the feature vector  
 331  $\mathbf{X}(n)$ . The meaning of “nearest neighbors” is generally interpreted in a Euclidean sense.  
 332 Therefore, if  $i$  belongs to  $S(\mathbf{X}, n)$  and  $j$  is not in  $S(\mathbf{X}, n)$ , then according to Euclidean  
 333 distance  $\|\mathbf{X}_n - \mathbf{X}_i\| \leq \|\mathbf{X}_n - \mathbf{X}_j\|$ . Intuitively speaking, the forecast  $x_{t+T+(m-1)\tau}^F$  in Eq. (14) is the  
 334 sample average of output rainfall of the  $K$  nearest neighbors to  $\mathbf{X}(n)$ . Obviously, a key task  
 335 is to determine the parameter  $K$  in the K-NN method.

336 **(4) ANN**

337 The multilayer perceptron network is by far the most popular ANN paradigm, which  
 338 usually uses the technique of error back propagation to train the network configuration. The  
 339 architecture of the ANN consists of a number of hidden layers and a number of neurons in  
 340 the input layer, hidden layers and output layer. ANNs with one hidden layer are commonly  
 341 used in hydrologic modeling (Dawson and Wilby, 2001; de Vos and Rientjes, 2005) since  
 342 these networks are considered to provide enough complexity to accurately simulate the  
 343 nonlinear-properties of the hydrologic process. Based on Eq. (13), the ANN forecasting  
 344 model is formulated as

$$345 \quad x_{t+T+(m-1)\tau}^F = f(\mathbf{X}_t, w, \theta, m, h) = \theta_0 + \sum_{j=1}^h w_j^{out} \varphi\left(\sum_{i=1}^m w_{ji} x_{t+(i-1)\tau} + \theta_j\right) \quad (15)$$



346 where  $\varphi$  denotes transfer functions;  $w_{ji}$  are the weights defining the link between the  $i$ th  
347 node of the input layer and the  $j$ th node of the hidden layer;  $\theta_j$  are biases associated to the  
348  $j$ th node of the hidden layer;  $w_j^{out}$  are the weights associated to the connection between the  
349  $j$ th node of the hidden layer and the node of the output layer; and  $\theta_0$  is the bias at the output  
350 node. To apply Eq. (15) to rainfall predictions, appropriate training algorithm is required to  
351 optimize  $w$  and  $\theta$ .

#### 352 (5) MANN

353 To construct MANN, the training data have to be divided into several clusters  
354 according to cluster analysis techniques, and then each single model is applied to each cluster.  
355 The FCM clustering technique is adopted in the present study (e.g., Bezdek, 1981, Wang et  
356 al., 2006). It is able to generate either soft or crisp clusters. ANN (or similar techniques) is  
357 unable to extrapolate beyond the range of the data used for training. Otherwise, poor  
358 forecasts or predictions can be expected when a new input data is outside the range of those  
359 used for training. Hard forecasting is, therefore, taken into consideration in this study.

360 Figure 3 displays the schematic diagram of MANN where the training data is  
361 partitioned into three clusters which are based on an assumption that three magnitudes of  
362 rainfall (i.e., low, medium, and high) may be derived from different mechanisms. According  
363 to this flow chart, once input-output pairs are obtained, they are first split into three subsets  
364 by the FCM technique, and then each subset is approximated by a single ANN. The final  
365 output of the modular model results directly from the output of one of three local models.

#### 366 2.4 Implementation framework of rainfall forecasting

367 Figure 4 illustrates the implementation framework of rainfall forecasting where four  
368 prediction models can be conducted in two modes: without/with three data preprocessing  
369 methods (dashed box). These acronyms in the column of “methods for model inputs”  
370 represent seven methods to determine model inputs: LCA (linear correlation analysis,  
371 Sudheer et al., 2002), AMI (average mutual information, Fraser and Swinney, 1986), PMI  
372 (partial mutual information, May et al., 2008), FNN (false nearest neighbors, Kennel et al.,  
373 1992), CI (correlation integral, Theiler, 1986), SLR, and MOGA (ANN based on multi-  
374 objective genetic algorithm, Giustolisi and Simeone, 2006).

## 375 **2.5 Evaluation of model performances**

376 The Pearson’s correlation coefficient ( $r$ ) or the coefficient of determination ( $R^2 = r^2$ ),  
377 have been identified as inappropriate measures in hydrologic model evaluation by Legates  
378 and McCabe (1999). The coefficient of efficiency (CE) (Nash and Sutcliffe, 1970) is a good  
379 alternative to  $r$  or  $R^2$  as a “goodness-of-fit” or relative error measure in that it is sensitive to  
380 differences in the observed and forecasted means and variances. Legates and McCabe (1999)  
381 also suggested that a complete assessment of model performance should include at least one  
382 absolute error measure (e.g., root mean square error (RMSE)) as necessary supplement to a  
383 relative error measure. Besides, the Persistence Index (PI) (Kitanidis And Bras, 1980) was  
384 adopted here for the purpose of checking the prediction lag effect. Three measures are  
385 therefore used in this study. They are listed below.

$$386 \quad CE = 1 - \frac{\sum_{i=1}^n (y_i - \hat{y}_i)^2}{\sum_{i=1}^n (y_i - \bar{y})^2} \quad (16)$$

$$387 \quad RMSE = \sqrt{\frac{1}{n} \sum_{i=1}^n (y_i - \hat{y}_i)^2} \quad (17)$$

388 
$$PI = 1 - \frac{\sum_{i=1}^n (y_i - \hat{y}_i)^2}{\sum_{i=1}^n (y_i - \bar{y})^2} \quad (18)$$

389 In these equations,  $n$  is the number of observations,  $\hat{y}_i$  stands for the forecasted flow,  
390  $y_i$  represents the observed flow,  $\bar{y}$  denotes the average observed flow, and  $y_{i-l}$  is the flow  
391 estimate from a so-call persistence model (or termed naïve model) that basically takes the last  
392 flow observation (at time  $i$  minus the lead time  $l$ ) as a prediction. CE and PI values of 1  
393 stands for perfect fits. A small value of PI may imply occurrence of lagged prediction.

### 394 **3. Applications of Models**

#### 395 **3.1 Determination of model inputs**

396 ANN, equipped with the Levenberg-Marquardt (L-M) training algorithm and  
397 hyperbolic tangent sigmoid transfer functions, is used as the benchmark model to examine  
398 aforementioned seven model input methods in terms of RMSE. Depending on the simplified  
399 algorithm from Yu et al. (2000) (downloaded at <http://small.eie.polyu.edu.hk/>), the four  
400 rainfall series are identified as non-chaotic since the correlation dimension does not display  
401 the property of convergence, in particular, for daily rainfall series. Results from remaining six  
402 methods are presented in Table 2. These results are based on one step lead prediction and let  
403  $X_{t+1}$  be the target value at one-step prediction horizon. It can be seen from RMSE that most  
404 of these methods tend to be mutually alternative because their RMSE are close. Owing to the  
405 convenience of operation, the LCA method is preferred in this study. Furthermore, Figure 5  
406 shows identification of effective inputs in Table 2 for the LCA method. Taking Wuxi and  
407 Zhenwan as examples, model inputs should take the previous 5-day and 7-day rainfalls for

408 them respectively because the partial auto-correlation function (PACF) value decays within  
409 the confidence band around these time lags.

### 410 **3.2 Identification of models**

411 The model identification is to determine the structure of a candidate model by using  
412 training data to optimize relevant parameters of model control once model inputs have been  
413 obtained. The LR model is built by the SLR technique. In terms of one step prediction  
414 (viz.,  $T = 1$ ), input variables can be found in Table 2. For example, the LR model for Wuxi  
415 can be expressed as

$$416 \quad x_{t+1}^F = 0.421x_t - 0.043x_{t-1} + 0.044x_{t-2} + 0.025x_{t-4} + 0.036x_{t-7} + 0.03x_{t-11} \quad (19)$$

417 With respect to K-NN, the model identification consists in finding the optimal  $K$  if the  
418  $m$ -dimensional input vector is determined. Sugihara and Mary (1990) suggested that the  
419 value of  $K$  was taken as  $K = m + 1$ . On the other hand, the choice of  $K$  should ensure the  
420 reliability of the forecasting (Fraser and Swinney, 1986). The check of robustness of  
421  $K = m + 1$  in terms of RMSE is presented in Figure 6, where  $K$  is in the interval of  $[2, 40]$ .  
422 Adopting the value of  $K$  as  $m + 1$  seems reasonable for the current study because the  
423 difference between its RMSE and the minimum RMSE is only 2.9% for Wuxi, 2.9% for  
424 Zhenwan, 2.6% for India, and 2.0% for Zhongxian, respectively. Consequently, the value of  
425  $K$  is 6 for Wuxi ( $m = 5$ ), 8 for Zhenwan ( $m = 7$ ), 13 for India ( $m = 12$ ), and 14 for  
426 Zhongxian ( $m = 13$ ), respectively.

427 Based on Eq. (14), the formula for one-step lead prediction in the context of K-NN  
428 can be defined as

$$429 \quad x_{t+1}^F = \frac{1}{K} \sum_{i=1}^K x_{t+1} \quad (20)$$

430 where  $X_{t+1}$  stands for an observed value associated with a neighbor of the current state. For a

431  $T$  – step lead prediction, Eq. (20) becomes

$$432 \quad x_{t+T}^F = \frac{1}{K} \sum_{i=1}^K x_{t+T} \quad (21)$$

433         The identification of ANN structure is to optimize the number of hidden nodes  $h$  in  
434 the hidden layer with the known model inputs and output. The optimal size  $h$  of the hidden  
435 layer is found by systematically increasing the number of hidden neurons from 1 to 10 until  
436 the network performance on the cross-validation set no longer improves significantly. Based  
437 on the L-M training algorithm and hyperbolic tangent transfer functions, the identified  
438 configurations of ANN are 5-5-1 for Wuxi, 7-4-1 for Zhenwan, 12-5-1 for India, and 13-3-1  
439 for Zhongxian, respectively. The same method is used to identify the structure of MANN, and  
440 the only difference is that the identification is repeated three times, with each time being for a  
441 local ANN. Consequently, MANN is obtained as 5-5/7/9-1 for Wuxi, 7-4/8/4-1 for Zhenwan,  
442 12-3/2/5-1 for India, and 13-1/1/1-1 for Zhongxian, respectively.

443         It is worthwhile to notice that the standardization/normalization of the training data is  
444 very crucial in the improvement of the model performance. Two methods can be found in the  
445 literature (Dawson and Wilby, 2001; Cannas et al., 2002; Rajurkar et al, 2002; Campolo et al.,  
446 2003; Wang et al., 2006). The standardization (also termed rescaling in some papers) method,  
447 as adopted above for model input determination, is to rescale the training data to  $[-1, 1]$ ,  $[0, 1]$   
448 or even more narrow interval depending on what kinds of transfer functions are employed in  
449 ANN. The normalization method is to rescale the training data to a Gaussian function with a  
450 mean of 0 and unit standard deviation, which is by subtracting the mean and dividing by the  
451 standard deviation. When the normalization approach is adopted, ANN uses the linear  
452 function (e.g. purelin) instead of the hyperbolic tangent sigmoid transfer function in the

453 output layer. In addition, some studies have indicated that considerations of statistical  
454 principles may improve ANN model performance (e.g. Cheng and Titterington, 1994). For  
455 example, the training data was recommended to be normally distributed (Fortin et al., 1997).  
456 Sudheer et al. (2002) suggested that the issue of stationarity should be considered in the ANN  
457 development because the ANN cannot account for trends and heteroscedasticity in the data.  
458 Their results showed that data transformation to reduce the skewness of data was capable of  
459 significantly improving the model performance. For the purpose of obtaining better model  
460 performance, four data-transformed schemes are examined:

- 461 • Standardizing the raw data (referred to as Std\_raw);
- 462 • Normalizing the raw data (referred to as Norm\_raw);
- 463 • Standardizing the n-th root transformed data (referred to as Std\_nth\_root);
- 464 • Normalizing the n-th root transformed data (referred to as Norm\_nth\_root).

465 Table 3 compares the ANN model performance of the four schemes in terms of  
466 RMSE and CE. The Norm\_raw scheme is, on the whole, slightly more effective than the  
467 Std\_raw method. It can also be seen that the effect of the n-th root scheme (3 is taken after  
468 trial and error) on the improvement of the performance is basically negligible. Therefore, the  
469 Norm\_raw scheme is adopted for the later rainfall prediction in the present study.

### 470 **3.3 Rainfall data preprocessing**

#### 471 **(1) MA**

472 The MA operation entails the window length  $k$  in Eq. (1) to smooth the raw rainfall  
473 data. An appropriate  $k$  can be found by systematically increasing  $k$  from 1 to 10. The  
474 smoothed data is then used to feed into each forecasting model. The targeted value of  $k$   
475 corresponds to the optimal model performance in terms of RMSE.

476 **(2) PCA**

477 PCA is employed in two ways: one for reduction of the dimensionality or preventing  
478 collinearity (depending on Eq. (2)); second for noise reduction by choosing leading  
479 components (contributing most of the variance of the original rainfall data) to reconstruct  
480 rainfall series (depending on Eq. (7)). The percentage  $V$  of total variance (see Eq. (6)) is set  
481 at three horizons, 85%, 90%, and 95% for principal component selection.

482 **(3) SSA**

483 This approach of filtering a time series to retain desired modes of variability is based  
484 on the idea that the predictability of a system can be improved by forecasting the important  
485 oscillations in time series taken from the system. The general procedure is to filter the  
486 original record first and then to build the forecasting model based on the filtered series. To  
487 filter the raw rainfall series, the series needs to be decomposed into components with the aid  
488 of SSA. The decomposition by SSA requires identifying the parameter pair  $(\tau, L)$ . The value  
489 of an appropriate  $L$  should be able to clearly resolve different oscillations hidden in the  
490 original signal. However, the present study does not require accurately resolving the raw  
491 rainfall signal into trends, oscillations, and noises. A rough resolution can be adequate for the  
492 separation of signals and noises where some leading eigenvalues should be identified.

493 To select  $L$ , a small interval of  $[3, 10]$  is examined in the present study. Figure 7  
494 shows the relation between singular spectrum (namely, a set of singular values) and singular  
495 number  $L$  for Wuxi, Zhenwan, India, and Zhongxian. It can be observed that the curve of  
496 singular values in each case except for Wuxi tends to level off with the increase of  $L$ .  
497 Generally, extraction of high-frequency oscillations becomes more difficult with the increase  
498 of singular number  $L$  (or mode).  $L$  is selected empirically by following the criterion that the

499 singular spectrum can be distinguished markedly under that  $L$ . According to this criterion,  
500  $L$  is set the value of 7 for India and Zhenwan, 6 for Zhongxian. For Wuxi, since all values in  
501 the interval satisfy the criterion, in order to reduce computational load in later filtering  
502 operation,  $L$  is set a small value of 5. The singular spectrum associated with the selected  $L$  is  
503 highlighted by the dotted solid line in Figure 7.

504 As regards  $\tau$ , Figure 8 presents the results of sensitivity analysis of singular spectrum  
505 on the lag time  $\tau$  using SSA with the determined  $L$ . For daily rainfall series, the singular  
506 spectrum can be distinguished only when  $\tau = 1$ . In contrast, the singular spectrum is  
507 insensitive to  $\tau$  in the case of monthly rainfall series. The final parameter pair ( $\tau, L$ ) in SSA  
508 are set as (1, 5) for Wuxi, (1, 7) for Zhenwan, (1, 7) for India, (1, 6) for Zhongxian,  
509 respectively.

### 510 **3.4 Filtering of RCs**

511 The subsequent task is to reconstruct a new rainfall series as model inputs by finding  
512 contributing RCs so as to improve the predictability of the rainfall series. There is no  
513 practical guide on how to identify a contributing or noncontributing component to the  
514 improvement of accuracy of prediction. Two proposed filtering methods, supervised and  
515 unsupervised, are herein examined.

#### 516 **(1) Supervised filtering (denoted by SSA1)**

517 Figure 9 depicts cross-correlation function (CCF) between RCs and the original  
518 Zhenwan rainfall series. The last plot in this figure presents the average of CCFs from all 7  
519 RCs. The average indicates an overall correlation between input and output at various lags  
520 (also termed prediction horizons). The plot of average CCF shows that the best correlation is  
521 positive and occurs at lag 1. Among all 7 RCs, RC1 exhibits the best positive correlation with



522 the original rainfall series. The CCF values for other RCs change alternatively between  
523 positive and negative with the increase of the lag. From the perspective of linear correlation,  
524 the positive or negative CCF value may indicate that the RC makes a positive or negative  
525 contribution to the output of model when the RC is used as the input of model. With the  
526 assumption, deleting RCs, which have negative correlations with the model output if the  
527 average CCF is positive, may improve the performance of the forecast model. This is the  
528 basic idea behind the supervised method.

529         The procedure of the supervised method coupled with ANN is depicted in Figure 10.  
530 The aim is to find the optimal  $p (\leq L)$  RCs from all  $L$  RCs for each prediction horizon. The  
531 procedure can be summarized into three steps: SSA decomposition, correlation coefficients  
532 sorting, and reconstructed components filtering. Operation in each step is bounded by the  
533 dashed box. It is worth noting that the filtering method is based on assumption that  
534 combination of components with the same sign in CCF (+ or -) can strengthen the correlation  
535 with the model output.

## 536 **(2) Unsupervised filtering (denoted by SSA2)**

537         There are some drawbacks on the supervised method. The salient one is that this  
538 method relies on linear correlation analysis, which disregards the existence of nonlinearity in  
539 meteorological processes. Also, random combinations among all RCs are not taken into  
540 account. To overcome these drawbacks, an unsupervised filtering method (also termed  
541 enumeration) is recommended where all input combinations are examined. There are  
542  $2^L$  combinations for  $L$  RCs. The unsupervised method may be computationally intensive if  
543  $L$  is large.

## 544 **4. Results and Discussions**

545 This section presents predictions using various models under two types of modes,  
546 namely “normal” and “data preprocessing”. The “data preprocessing” mode is separately  
547 described by MA, PCA, and SSA. To extend one-step-ahead prediction to multi-step-ahead  
548 prediction, a direct multi-step prediction method (by directly having the multi-step-ahead  
549 prediction as output, also termed static prediction method) is adopted in this study to perform  
550 two- and three-step-ahead predictions.

### 551 **4.1 Forecasting with normal mode**

552 Table 4 shows results of three prediction horizons by applying five models including  
553 naïve model to each case study. The naïve model is used as the benchmark in which the  
554 forecasted value is directly equal to the last observed value (namely, no change). The naïve  
555 model presents the poorest forecasting which can be explained by the fact that it is unlikely to  
556 capture any dependence relation. From the perspective of rainfall series, the monthly rainfall  
557 can be better predicted than the daily rainfall. Generally, a daily rainfall series, in particular  
558 in a semi-humid and semi-dry or dry region, tends to be intermittent and discontinuous due to  
559 a large number of no rain periods (dry periods). Two global modeling methods, LR and ANN,  
560 mainly capture the zero-zero (or similar extreme low-intensity) rainfall patterns in daily  
561 rainfall series because the type of pattern is overwhelmingly dominant in the daily rainfall  
562 series. As a consequence, poor performance indices in terms of RMSE, CE, and PI can be  
563 observed (depicted in Table 4 for Wuxi and Zhenwan). Nevertheless, Table 4 also shows that  
564 MANN performs the best in each case study. MANN adopts three local ANN models, one for  
565 each cluster generated by FCM, which can better capture the mapping relation than using a  
566 single global ANN. It can be noticed that MANN is more effective for daily rainfall series

567 than monthly rainfall data, which can be because daily rainfall data is more irregular (or non-  
568 periodic) than monthly rainfall series. The use of K-NN for daily rainfall forecasting is even  
569 worse than LR although it employs a local prediction approach. Apart from the issue of the  
570 selection of  $K$ , the performance of K-NN is also influenced by the similarity of input-output  
571 patterns. The smooth monthly rainfall series easily construct similar patterns so that they are  
572 well predicted by K-NN. It is worth noting that negative values occasionally appear in the  
573 forecasts of ANN or MANN whereas this situation does not happen in the K-NN method.

574         Take Wuxi and India data as representative examples, Figure 11 shows the scatter  
575 plots and hyetographs of the results at one-day-ahead prediction of ANN and MANN using  
576 the rainfall data of Wuxi, where the hyetograph is plotted in a selected range for better visual  
577 inspection. ANN seriously underestimates a number of moderate- and high-intensity rainfalls.  
578 The low values of CE and PI demonstrate that time shift between the forecasted and observed  
579 rainfall may occur, which is further verified by the hyetograph. MANN improves noticeably  
580 the accuracy of forecasting in terms of CE and PI. As shown by the scatter plots, the  
581 medium-intensity rainfall can be simulated better by MANN although high-intensity rainfalls  
582 (or peak values) are still underestimated. Figure 12 shows scatter plots and hyetographs of  
583 results at one-day-ahead prediction of ANN and MANN using the rainfall data of India. It  
584 can be seen from hyetograph graphs that both ANN and MANN reproduce well the  
585 corresponding observed rainfall data, which is further revealed by the scatter plots with a low  
586 dispersion around the exact fit line.

587         Figure 13 shows the analysis of the lag effect between forecasted and observed  
588 rainfall series. The value of CCF at zero lag corresponds to the actual performance (i.e.  
589 correlation coefficient) of the model. A target lag is associated with the maximum value of

590 CCF, and is an expression for the mean lag for the forecast. It can be seen from Figure 16  
591 that ANN makes fairly obvious lagged predictions for daily rainfall series, and the lag effect  
592 can be overcome by MANN. There are 1, 2, and 3 days lag for Wuxi, which are respectively  
593 associated with one-, two-, and three-day-ahead forecasting. In contrast, there is no lag effect  
594 in monthly rainfall predictions of ANN or MANN.

#### 595 **4.2 Forecasting with MA**

596 Table 5 presents forecasted results of ANN with the “backward” MA (hereafter  
597 referred to as ANN-MA) using the Wuxi rainfall data. The performance indices  
598 corresponding to  $k=1$  are associated with the normal ANN. Results at each prediction  
599 horizon seem to be insensitive to the window length  $k$  in view of slight differences among  
600 each performance index for  $k$  from 1 to 10. Considering the fact that ANNs tend to generate  
601 unstable outputs, the influence of MA on the performance of ANN is negligible. Small values  
602 of PI also imply that MA cannot eliminate the lagged forecast from ANN.

#### 603 **4.3 Forecasting with PCA**

604 As mentioned previously, PCA is used in two ways: one (denoted by PCA1) for  
605 reduction of dimensionality (also termed principal component regression) and the other one  
606 (denoted by PCA2) for noise reduction. Results from PCA1 are presented in Table 6. The  
607 scenario of  $V=100\%$  stands for forecasting using models with the normal mode. Results  
608 show that PCA1 cannot improve the model performances in terms of RMSE, CE, and PI,  
609 which means that the reduction of dimensionality is unnecessary for the present case studies.  
610 Actually, the original inputs are characterized by a low dimension. Table 7 describes the  
611 results from PCA2. According to results from LR and K-NN (because results from ANN tend  
612 to be unstable), a marginal improvement in the model performances can be observed for the

613 Wuxi watershed whereas the model performances deteriorate for the India watershed with the  
614 decrease of the value of  $V$ .

#### 615 **4.4 Forecasting with SSA**

616 Following the procedure in Figure 10, the supervised filtering (SSA1) using ANN for  
617 RCs of Wuxi and India is illustrated in Figure 14. The RMSE associated with the maximum  
618 number of  $p$  (for instance  $p=5$  for Wuxi) represents the performance of ANN with the  
619 normal mode. The optimal  $p$  corresponds to the minimum RMSE, which can be found by  
620 systematically deleting RCs one at a time. Consequently, numbers of chosen optimal  $p$  RCs  
621 in three forecasting horizons are 3, 2, and 1 for Wuxi, and 1, 3, and 5 for India, respectively.  
622 However, the unsupervised filtering method (SSA2) is based on enumeration of combinations  
623 of all RCs. Selection of the optimal  $p$  RCs cannot be presented in a graphical form.

624 Table 8 shows selected  $p$  at various prediction horizons using LR, K-NN, and ANN  
625 in conjunction with SSA1 and SSA2. A large amount of information can be extracted from  
626 this Table. First of all, a considerable improvement in the model performance is achieved by  
627 each forecasting model in conjunction with SSA1 or SSA2, compared with results in Table 4.  
628 From the perspective of rainfall series, the accuracy of daily rainfall prediction is improved  
629 significantly in comparison to that in the normal mode. Secondly, as expected, results from  
630 SSA2 are superior to or at least equivalent to those from SSA1 since the former examines  
631 each combination of RCs in search of the optimal  $p$ . SSA2 is therefore considered as an  
632 efficient and effective method if the number  $L$  of RCs is small. For the present four cases,  
633 SSA2 method is appropriate due to the small number of RCs. Once  $L$  is large, say 40 or 50,  
634 SSA1 may be a good alternative where a relative optimal forecasting can be guaranteed.

635 Additionally, it should be noted that the optimal  $p$  are different at three forecast horizons.  
636 Finally, Table 8 also shows that, among the three models, ANN performs the best with SSA1  
637 or SSA2, which is consistent with results in the normal mode.

638 In the normal mode, MANN has been proved to be superior to ANN, in particular, for  
639 daily rainfall forecasting. As an attempt to improve the accuracy of rainfall forecasting,  
640 MANN is also coupled with SSA2. Table 9 demonstrates results in terms of RMSE, CE, and  
641 PI using MANN compared with those of ANN. Good accuracies of forecasting are made by  
642 both MANN and ANN. It can be seen from values of PI that the prediction lag effect is  
643 completely eliminated. The model performance does not deteriorate markedly with the  
644 increase of the forecasting lead. Results also show that MANN still maintains a salient  
645 superiority over ANN in the SSA2 mode for both daily and month rainfall series.

646 One-step lead estimates of MANN and ANN with the help of SSA2 are shown in  
647 Figure 15 (Wuxi) and Figure 16 (India) in the form of hyetographs and scatter plots (the  
648 former is plotted in a selected range for better visual inspection). Compared with Figure 11,  
649 each scatter plot in Figure 15 is closer to the exact line, which means that the daily rainfall  
650 process is fitted appropriately. Nevertheless, some peak values still remain mismatched  
651 although MANN shows a better ability to capture the peak value than ANN. Regarding the  
652 monthly rainfall series, the scatter plots with perfect match of the diagonal indicates that the  
653 rainfall process is perfectly reproduced. The representative hyetograph shows that the peak  
654 times and peak values are also accurately predicted.

655 Figure 17 presents the correlation analysis between observed and forecasted rainfall  
656 from ANN and MANN using the Wuxi and India series, respectively. Compared with Figure

657 13, the lagged prediction of ANN is completely eliminated by SSA2 since the maximum  
658 CCF occurs at zero lag. The larger the CCF at zero lag is, the better the model performance is.

#### 659 **4.5 Discussions**

660 Some discussions regarding forecasting models and the effects of the SSA technique  
661 are made in the following.

##### 662 **(1) About the investigation of effects of SSA**

663 Figure 18 shows that a large number of zeros and near zeros occur in the original  
664 Wuxi rainfall which makes the series discontinuous. Using the intermittent series is difficult  
665 to reconstruct similar input patterns for a forecasting model. Thus, depending on those  
666 reconstructed input patterns, data-driven models based on pattern training, for example,  
667 ANNs, tend to be unfeasible. In contrast, rainfall series preprocessed by SSA becomes  
668 smoother where most of zeros are replaced by nonzero values. New input vectors from the  
669 reconstructed rainfall series are characterized by better repetition of patterns so that they are  
670 easier reproduced.

671 To investigate the influence of SSA on the ANN's performance, correlation analyses  
672 between inputs and output of ANN and ANN-SSA2 are compared using the Wuxi data and  
673 are depicted in Figure 19. As the input and output series in ANN are both the raw rainfall  
674 series, the cross-correlation analysis is equivalent to the autocorrelation analysis of the raw  
675 rainfall series. At all three prediction horizons, cross-correlation coefficients (CCs) between  
676 reconstructed inputs by SSA2 and the raw rainfall data are improved significantly at most  
677 lags except for the lag of 3 at one-step lead. It should be recalled that model inputs are the  
678 previous five rainfall data for Wuxi. The "starting point" in Figure 19 represents the first  
679 previous rainfall of the five inputs, and the remaining inputs consist of four points after the

680 starting point. It can be observed that the CCF value between each new model input and  
681 output are far larger than that between the raw model input and output (seen at the same lag).  
682 Therefore, the improvement of a model's performance by the SSA technique may be owing  
683 to the enhancement of the mapping relation of model input and output by deleting noises  
684 hidden in the raw signals.

685 **(2) About parameter  $L$  in SSA**

686 The parameter  $L$  in SSA has a significant impact on the performance of a forecasting  
687 model since the optimal  $p$  RCs may be different with the change of  $L$  when using the same  
688 forecasting model at the same prediction horizon. The selection of  $L$  in this study is based on  
689 the interval of [3, 10] in conjunction with an empirical criterion (namely, a particular  $L$  is  
690 selected only if the singular spectrum can be distinguished markedly under that  $L$ ). To check  
691 the robustness of the empirical method, each  $L$  in [3, 10] is examined by the LR model with  
692 SSA2 using the Wuxi and Zhenwan data and presented in Table 10. As mentioned previously,  
693 the target  $L$  for Wuxi and Zhenwan are 5 and 7, respectively. The RMSE associated with  
694 them at each prediction horizon is highlighted in bold (shown in Table 10). In terms of Wuxi,  
695 the difference between the target RMSE and the minimum RMSE at the same prediction  
696 horizon is only 9.2% for one-step prediction, 1.4% for two-step prediction, 0.0% for three-  
697 step prediction, respectively. Regarding Zhenwan, the three values are respectively 5.2%,  
698 7.5%, and 0.0%. These changes are slight and cannot influence the conclusions drawn  
699 previously. Therefore, the empirical method for the present rainfall data should be  
700 appropriate.



701 **5. Conclusion**

702 This study suggests the use of modular artificial neural network (MANN) coupled  
703 with data preprocessing techniques for improving four rainfall predictions from India and  
704 China consisting of two monthly and two daily series. To reasonably evaluate MANN's  
705 performance, three models, LR, K-NN and ANN, are used for the purpose of comparison. In  
706 the process of model development, model inputs and data preprocessing techniques are  
707 carefully analyzed and discussed. The following conclusions are reached based on this study:

708 1. LCA is regarded as an effective and efficient method among all seven input  
709 techniques due to its simplicity of computation and comparable capability of forecasting.

710 2. In the normal mode (without data preprocessing), MANN distinguishes from the  
711 other three models for both monthly and daily rainfall series forecasting. Whilst all four  
712 models reasonably forecast two monthly rainfall series, only MANN is able to simulate each  
713 daily rainfall series without obvious lag effect.

714 3. In the data preprocessing mode, the effect of MA is negligible for the improvement  
715 of each forecasting model.

716 4. PCA as a data preprocessing technique is discussed in two forms, i.e. PCA1 for the  
717 purpose of dimension reduction, and PCA2 for the purpose of noise reduction. Results show  
718 that PCA1 cannot improve model's performance and PCA2 marginally improve model's  
719 performance.

720 5. Two filtering method, i.e. supervised (SSA1) and unsupervised (SSA2), are  
721 examined for SSA when coupled with forecasting models. It can be found that each model  
722 achieves considerable improvement in performance with the aid of SSA1 or SSA2. In terms  
723 of forecasting models, MANN still outperforms all other models.

---

724 6. As far as two filtering methods are concerned, SSA2 tends to be better if the  
725 number of raw RCs is small. Otherwise, SSA1 is a good alternative.

726 7. A further discussion reveals that the essence of SSA in improving model  
727 performance is to strengthen the mapping relation of model input and output by deleting  
728 noises in the raw signal.

729 8. There is still considerable room for improving forecasting of peak values although  
730 MANN coupled with SSA has made perfect overall predictions for daily rainfall series.

731

732 **Nomenclature**

733	ACF	Auto Correlation Function
734	AMI	Average Mutual Information
735	ANN	Artificial Neural Networks
736	CC	Cross-correlation Coefficient
737	CCF	Cross Correlation Function
738	CE	Coefficient of Efficiency
739	CI	Correlation Integral
740	FCM	Fuzzy C-means
741	FNN	False Nearest Neighbor
742	K-NN	K-Nearest-Neighbors
743	LCA	Linear Correlation Analysis
744	L-M	Levenberg-Marquart
745	LR	Linear Regression
746	MA	Moving Average

---

747	MANN	Modular Artificial Neural Networks
748	MOGA	ANN based on Multi-objective Genetic Algorithm
749	PACF	Partial Auto Correlation Function
750	PC	Principal Component
751	PCA	Principal Component Analysis
752	PMI	Partial Mutual Information
753	PI	Persistence Index
754	RC	Reconstructed Component
755	RMSE	Root Mean Square Error
756	SLR	Stepwise Linear Regression
757	SSA	Singular Spectrum Analysis
758	SVD	Singular Value Decomposition
759	SVM	Support Vector Machine
760	SVR	Support Vectors Regression
761	WA	Wavelet Analysis

762

763 **References:**

764 Abrahart, R.J. and See, L.M. (2002), Multi-model data fusion for river flow forecasting: an  
765 evaluation of six alternative methods based on two contrasting catchments. *Hydrology and*  
766 *Earth System Sciences*, 6(4), 655-670.

767 Baratta et al., Baratta, D., Cicioni, G., Masulli, F. and Studer, L. (2003), Application of an  
768 ensemble technique based on singular spectrum analysis to daily rainfall forecasting. *Neural*  
769 *Networks*, 16, 375-387.

- 770 Bezdek, J.C. (1981), *Pattern Recognition with Fuzzy Objective Function Algorithms*. Plenum  
771 Press, New York.
- 772 Brath, A., Montanari, A., and Toth, E. (2002), Neural networks and non-parametric methods  
773 for improving realtime flood forecasting through conceptual hydrological models. *Hydrology  
774 and Earth System Sciences*, 6(4), 627-640.
- 775 Campolo, M., Andreussi, P. and Soldati, A. (2003), Artificial neural network approach to  
776 flood forecasting in the river Arno. *Hydrological Sciences Journal*, 48(3), 381-398.
- 777 Cannas, B., Fanni, A., Pintus, M., and Sechi, G. M. (2002), Neural Network Models to  
778 Forecast Hydrological Risk. *IEEE IJCNN*, 2002.
- 779 Chan, J.C.L., and Shi, J.E. (1999), Prediction of the summer monsoon rainfall over South  
780 China. *International Journal of Climatology*, 19 (11), 1255-1265.
- 781 Chattopadhyay, S., and Chattopadhyay, G. (2007), Identification of the best hidden layer size  
782 for three-layered neural net in predicting monsoon rainfall in India. *Journal of  
783 Hydroinformatics*, 10(2), 181-188.
- 784 Cheng, B., and Titterton, D. M. (1994), Titterton Neural networks: A review from a  
785 statistical perspective. *Statistical Science*, 9(1), 2-54.
- 786 Chu, P.S., and He, Y.X. (1994), Long-Range Prediction of Hawaiian Winter Rainfall Using  
787 Canonical Correlation-Analysis). *International Journal of Climatology*, 14(6), 659-669.
- 788 Corzo, G., and Solomatine, D. (2007), Baseflow separation techniques for modular artificial  
789 neural network modelling in flow forecasting. *Hydrological Sciences–Journal–des Sciences  
790 Hydrologiques*, 52(3), 491-507.

- 791 Coulibaly, P., Haché, M., Fortin, V., and Bobée, B. (2005), Improving daily reservoir inflow  
792 forecasts with model combination. *Journal of Hydrologic Engineering*, 10(2), 91-99.
- 793 Dawson, C.W., and Wilby, R.L. (2001), Hydrological Modeling Using Artificial Neural  
794 Networks. *Progress in Physical Geography*, 25(1), 80-108.
- 795 DelSole, T., and Shukla, J. (2002), Linear prediction of Indian monsoon rainfall. *Journal of*  
796 *Climate*, 15 (24), 3645-3658.
- 797 de Vos, N.J. and Rientjes, T.H.M. (2005), Constraints of artificial neural networks for rainfall  
798 -runoff modeling: trade-offs in hydrological state representation and model evaluation.  
799 *Hydrology and Earth System Sciences*, 9, 111-126.
- 800 Diomede, T., Davolio, S., Marsigli, C., Miglietta, M. M., Moscatello, A., Papetti, P.,  
801 Paccagnella, T., Buzzi, A., and Malguzzi, P. (2008), Discharge prediction based on multi-  
802 model precipitation forecasts. *Meteorology and Atmospheric Physics*, 101 (3-4), 245-265.
- 803 Draper, N. R. and Smith, H. (1998), *Applied regression analysis*, 3rd ed. New York: Wiley.
- 804 Fortin, V., Ouarda, T.B.M.J., and Bobe'e, B., (1997), Comment on 'The use of artificial  
805 neural networks for the prediction of water quality parameters' by H.R. Maier and G.C.  
806 Dandy. *Water Resources Research*, 33 (10), 2423-2242.
- 807 Fraser, A.M. and Swinney, H.L. (1986), Independent coordinates for strange attractors from  
808 mutual information, *Physical Review A*, 33(2), 1134-1140.
- 809 Ganguly, A.R., and Bras, R.L. (2003), Distributed quantitative precipitation forecasting  
810 (DQPF) using information from radar and numerical weather prediction models. *Journal of*  
811 *Hydrometeorology*, 4 (6), 1168-1180.

- 812 Giustolisi, O., and Savic, D. A. (2006), A symbolic data-driven technique based on  
813 evolutionary polynomial regression, *Journal of Hydroinformatics*, 8(3), 207-222.
- 814 Golyandina, N. Nekrutkin, V., and Zhigljavsky, A. (2001), *Analysis of Time Series Structure:*  
815 *SSA and Related Techniques*, Chapman & Hall/CRC.
- 816 Guhathakurta, P. (2008), Long lead monsoon rainfall prediction for meteorological sub-  
817 divisions of India using deterministic artificial neural network model. *Meteorology and*  
818 *Atmospheric Physics*, 101 (1-2), 93-108.
- 819 Guhathakurta, P., Rajeevan, M., and Thapliyal, V. (1999), Long range forecasting Indian  
820 summer monsoon rainfall by a hybrid Principal Component neural network model.  
821 *Meteorology and atmospheric physics*, 71, (3-4), 255-266.
- 822 Hsu, K.L., Gupta, H.V., Gao, X.G., Sorooshian, S., and Imam, B. (2002), Self-organizing  
823 linear output map (SOLO): An artificial neural network suitable for hydrologic modeling and  
824 analysis. *Water Resources Research*, 38(12), 1302, doi:10.1029/2001WR000795.
- 825 Hu, T.S., Lam, K.C., Ng, S.T., (2001), River flow time series prediction with a range-  
826 dependent neural network. *Hydrological Science Journal*, 46 (5), 729-745.
- 827 Hotelling, H., (1933), Analysis of a complex of statistical variables into principal components.  
828 *Journal of Educational Psychology*, 24, 417-441.
- 829 Hu, T.S., Wu, F.Y., and Zhang, X. (2007), Rainfall-runoff modeling using principal  
830 component analysis and neural network. *Nordic Hydrology*, 38(3), 235-248.
- 831 Jain, A., and Srinivasulu, S. (2006), Integrated approach to model decomposed flow  
832 hydrograph using artificial neural network and conceptual techniques. *Journal of Hydrology*,  
833 317, 291-306.

- 
- 834 Jayawardena, A.W., and Lai, F. (1994), Analysis and prediction of chaos in rainfall and  
835 stream flow time series. *Journal of hydrology*, 153, 23-52.
- 836 Kennel, M. B., Brown, R., and Abarbanel, H. D. I. (1992), Determining embedding  
837 dimension for phase space reconstruction using geometrical construction. *Physical Review A.*,  
838 45(6), 3403-3411.
- 839 Kim, T., Heo, J. H. and Jeong, C. S. (2006), Multireservoir system optimization in the Han  
840 River basin using multi-objective genetic algorithms. *Hydrological Processes*, 20 (9), 2057-  
841 2075.
- 842 Kitanidis, P. K. and Bras, R. L. (1980), Real-time forecasting with a conceptual hydrologic  
843 model, 2, applications and results, *Water Resources Research*, 16 (6), 1034–1044.
- 844 Lee, C.F., Lee, J.C. and Lee, A.C., (2000), *Statistics for business and financial economics*  
845 (2nd version), World Scientific, Singapore.
- 846 Legates, D. R., and McCabe, Jr, G. J. (1999), Evaluating the use of goodness-of-fit measures  
847 in hydrologic and hydroclimatic model validation, *Water Resources. Research*, 35(1), 233-  
848 241.
- 849 Li, F., and Zeng, Q.C. (2008), Statistical prediction of East Asian summer monsoon rainfall  
850 based on SST and sea ice concentration. *Journal of the meteorological society of Japan*, 86  
851 (1), 237-243.
- 852 Lin, G.F., and Chen, L.H. (2005), Application of artificial neural network to typhoon rainfall  
853 forecasting. *Hydrological Processes*, 19 (9), 1825-1837.
- 854 Lin, G.F., Chen, G.R., Wu, M.C., and Chou, Y.C. (2009), Effective forecasting of hourly  
855 typhoon rainfall using support vector machines. *Water Resources Research*, 45, W08440.

856 doi:10.1029/2009WR007911.

857 Lin, G.F., and Wu, M.C. (2009), A hybrid neural network model for typhoon-rainfall  
858 forecasting. *Journal of Hydrology*, 375 (3-4), 450-458.

859 Lisi, F., Nicolis, and Sandri, M. (1995), Combining singular-spectrum analysis and neural  
860 networks for time series forecasting. *Neural Processing Letters*, 2(4), 6-10.

861 Marques, C.A.F., Ferreira, J., Rocha, A., Castanheira, J., Gonçalves, P., Vaz, N., and Dias,  
862 J.M. (2006), Singular spectral analysis and forecasting of hydrological time series. *Physics  
863 and Chemistry of the Earth*, 31, 1172-1179.

864 May, R.J., Maier, H.R., Dandy, G.C., and Fernando, T.M.K. (2008), Non-linear variable  
865 selection for artificial neural networks using partial mutual information. *Environmental  
866 Modeling & Software*, 23, 1312-1328.

867 McCuen, R. H. (2005), *Hydrologic analysis and design* (3rd ed.), Upper Saddle River, NJ:  
868 Pearson/Prentice Hall.

869 Munot, A. A., and Kumar, K.K. (2007), Long range prediction of Indian summer monsoon  
870 rainfall. *Journal of Earth System Science*, 116 (1), 73-79.

871 Nash, J. E. and Sutcliffe, J. V. (1970), River flow forecasting through conceptual models part  
872 I — A discussion of principles. *Journal of Hydrology*, 10 (3), 282-290.

873 Nayagam, L.R., Janardanan, R., and Mohan, H.S.R. (2008), An empirical model for the  
874 seasonal prediction of southwest monsoon rainfall over Kerala, a meteorological subdivision  
875 of India. *International Journal of Climatology*, 28 (6), 823-831.

876 Newbold, P., Carlson, W. L., and Thorne, B.M. (2003), *Statistics for business and economics*



- 877 (fifth version), Prentice Hall, Upper Saddle River, N.J.
- 878 Partal, T. and Kişi, Ö. (2007), Wavelet and Neuro-fuzzy conjunction model for precipitation  
879 forecasting. *Journal of Hydrology*, 342 (2), 199-212.
- 880 Pearson, K., (1901), On lines and planes of closest fit to systems of points in space.  
881 *Philosophical Magazine*, 2, 559-572.
- 882 Pongracz, R., Bartholy, J., and Bogardi, I. (2001), Fuzzy rule-based prediction of monthly  
883 precipitation. *Physics and Chemistry of the Earth Part B-Hydrology Oceans and Atmosphere*,  
884 26 (9), 663-667.
- 885 Rajurkar, M.P., Kothyari, U.C., and Chaube, U.C. (2002), Artificial neural networks for daily  
886 rainfall-runoff modeling. *Hydrological Sciences-Journal*, 47(6), 865-876.
- 887 Salas, J.D., Delleur, J.W., Yevjevich, V., and Lane, W.L. (eds) (1985), *Applied Modeling of*  
888 *Hydrologic Time Series*. Water Resources Publications: Littleton, Colorado.
- 889 See, L., and Openshaw, S. (2000), A hybrid multi-model approach to river level forecasting.  
890 *Hydrology Science Journal*, 45(4), 523-536.
- 891 Shamseldin, A.Y. and O'Connor, K.M. (1999), A real-time combination method for the  
892 outputs of different rainfall-runoff models. *Hydrological Sciences Journal*, 44(6), 895-912.
- 893 Shamseldin, A.Y., O'Connor, K.M. and Liang, G.C., (1997), Methods for combining the  
894 outputs of different rainfall runoff models, *Journal of Hydrology*, 197, 203–229.
- 895 Sheng, C., Gao, S., and Xue, M. (2006), Short-range prediction of a heavy precipitation event  
896 by assimilating Chinese CINRAD-SA radar reflectivity data using complex cloud analysis.  
897 *Meteorology and Atmospheric Physics*, 94 (1-4), 167-183.

- 898 Shrestha, D.L., and Solomatine, D.P. (2006), Machine learning approaches for estimation of  
899 prediction interval for the model output. *Neural Networks*, 19(2), 225-235.
- 900 Silverman, D., and Dracup, J.A. (2000), Artificial neural networks and long-range  
901 precipitation in California. *Journal of Applied Meteorology* 31 (1), 57-66.
- 902 Sivapragasam, C., and Liong, S. Y. (2005), Flow categorization model for improving  
903 forecasting. *Nordic Hydrology* 36 (1), 37-48.
- 904 Sivapragasam, C., Liong, S.Y. and Pasha, M.F.K. (2001), Rainfall and runoff forecasting with  
905 SSA-SVM approach. *Journal of Hydroinformatics*, 3(7), 141-152.
- 906 Sivapragasam, C., Vincent and, P., and Vasudevan, G. (2007), Genetic programming model  
907 for forecast of short and noisy Data. *Hydrological Processes*, 21, 266-272.
- 908 Solomatine, D. P., and Ostfeld, A. (2008), Data-driven modelling: Some past experiences and  
909 new approaches. *Journal of Hydroinformatics*, 10(1), 3-22.
- 910 Solomatine, D. P. and Xue, Y. I. (2004), M5 model trees and neural networks: application to  
911 flood forecasting in the upper reach of the Huai River in China. *Journal of Hydrological  
912 Engineering*, 9(6), 491-501.
- 913 Sudheer, K. P., Gosain, A. K., and Ramasastri, K. S. (2002), A data-driven algorithm for  
914 constructing artificial neural network rainfall-runoff models. *Hydrological Processes*, 16,  
915 1325-1330.
- 916 Sugihara, G and May, R.M. (1990), Nonlinear forecasting as a way of distinguishing chaos  
917 from measurement error in time series. *Nature*, 344, 734- 741.
- 918 Sudheer, K. P., Gosain, A. K., and Ramasastri, K. S. (2002), A data-driven algorithm for

- 
- 919 constructing artificial neural network rainfall-runoff models. *Hydrological Processes*, 16,  
920 1325-1330.
- 921 Theiler, J., (1986), Spurious dimension from correlation algorithms applied to limited time-  
922 series data. *Physical Review A*, 34 (3), 2427-2432.
- 923 Toth, E, Brath, A., and Montanari, A. (2000), Comparison of short-term rainfall prediction  
924 models for real-time flood forecasting. *Journal of Hydrology*, 239, 132-147.
- 925 Venkatesan, C., Raskar, S.D., Tambe, S.S., Kulkarni, B.D., and Keshavamurty, R.N. (1997),  
926 Prediction of all India summer monsoon rainfall using error-back-propagation neural  
927 networks. *Meteorology and Atmospheric Physics*, 62 (3-4), 225-240.
- 928 Wang, W., Van Gelder, P.H.A.J.M., Vrijling, J.K. and Ma, J. (2006), Forecasting Daily  
929 Streamflow Using Hybrid ANN Models. *Journal of Hydrology*, 324, 383-399.
- 930 Wu, C.L., Chau, K.W., and Li, Y.S., (2009), Methods to improve neural network performance  
931 in daily flows prediction. *Journal of Hydrology*, 372(1-4), 80-93.
- 932 Wu, C.L., Chau, K.W. and Li, Y.S. (2008), River stage prediction based on a distributed  
933 support vector regression. *Journal of Hydrology*, 358, 96-111.
- 934 Xiong, L.H., Shamseldin, A.Y., and O'Connor, K.M. (2001), A non-linear combination of  
935 forecasts of rainfall-runoff models by the first-order TS fuzzy system for forecast of rainfall-  
936 runoff model. *Journal of Hydrology*, 245, 196-217.
- 937 Yates, D.N., Warner, T.T., and Leavesley, G.H. (2000), Prediction of a flash flood in complex  
938 terrain. Part II: A comparison of flood discharge simulations using rainfall input from radar, a  
939 dynamic model, and an automated algorithmic system. *Journal of Applied Meteorology*, 39  
940 (6), 815-825.

- 
- 941 Yu, D.L., Gomm, J.B., and Williams, D. (2000), Neural model input selection for a MIMO  
942 chemical process. *Engineering Applications of Artificial Intelligence*, 13(1), 15-23.
- 943 Zhang, B., and Govindaraju, R. S. (2000), Prediction of watershed runoff using Bayesian  
944 concepts and modular neural networks. *Water Resources Research*, 36(3), 753-762.
- 945

946 **Figure Captions**

947 Figure 1. Location of Daning river basin (Map of Chongqing in the left panel, and Daning  
948 watershed in the dashed box)

949 Figure 2. Rainfall series of (a) Wuxi, (b) India, (c) Zhenwan, and (d) Zhongxian

950 Figure 3. Flow chart of hard forecasting using a modular model

951 Figure 4. Implementation framework of forecast models with/without data preprocessing

952 Figure 5. Plots of ACF and PACF of the rainfall series with the 95% confidence bounds (the  
953 dashed lines), (a) and (c) for Wuxi, and (b) and (d) for Zhenwan

954 Figure 6. Check of robustness of  $K$  in KNN method for (a) Wuxi, (b) India, (c) Zhenwan,  
955 and (d) Zhongxian.

956 Figure 7. Singular Spectrum as a function of lag using various window lengths  $L$  for (a) Wuxi,  
957 (b) India, (c) Zhenwan, and (d) Zhongxian

958 Figure 8. Sensitivity analysis of singular Spectrum on varied  $\tau$  for (a) Wuxi, (b) India, (c)  
959 Zhenwan, and (d) Zhongxian

960 Figure 9. Plots of CCF between each RC and the raw rainfall data for Zhenwan

961 Figure 10. Supervised procedure for a forecast model with SSA

962 Figure 3. Scatter plots and hyetographs of one-step-ahead forecast using ANN and MANN  
963 for Wuxi ((a) and (c) from ANN, and (b) and (d) from MANN)

964 Figure 4. Scatter plots and hyetographs of one-step-ahead forecast using ANN and MANN  
965 for India ((a) and (c) from ANN, and (b) and (d) from MANN)

966 Figure 5. CCFs at three forecast horizons for various lags in time of observed and forecasted  
967 rainfall of ANN and MANN: Wuxi (left column) and India (right column)

968 Figure 6. Performance of ANN with SSA1 in terms of RMSE as a function of  $p$  ( $\leq L$ )

969 selected RCs at various prediction horizons: (a) Wuxi and (b) India  
970 Figure 7. Scatter plots and hyetographs of one-step-ahead forecast using ANN and MANN  
971 with SSA2 for Wuxi ((a) and (c) from ANN, and (b) and (d) from MANN)  
972 Figure 8. Scatter plots and hyetographs of one-step-ahead forecast using ANN and MANN  
973 with SSA2 for India ((a) and (c) from ANN, and (b) and (d) from MANN)  
974 Figure 17. CCFs at three forecast horizons using ANN and MANN with Wuxi and India ((a)  
975 and (c) for Wuxi and (b) and (d) for India)  
976 Figure 18. Hyetographs (detail; from 900<sup>th</sup> to 950<sup>th</sup>) of Wuxi: (1) the raw rainfall series and (2)  
977 reconstructed rainfall series for one-step prediction of ANN.  
978 Figure 19. CCF between inputs and output for ANN and ANN-SSA2 at three prediction  
979 horizons using the Wuxi data  
980

981 **Table captions**

982 Table 1. Pertinent information for four watersheds and the rainfall data

983 Table 2. Comparison of methods to determine mode inputs using ANN model

984 Table 3. Performance comparison of ANN with different data-transformed methods

985 Table 4. Model performances at three forecasting horizons under normal mode

986 Table 5. Model performances of ANN-MA using the Wuxi data

987 Table 6. Multiple-step predictions for Wuxi and India series using LR, K-NN, and ANN with

988 PCA1

989 Table 7. Multiple-step predictions for Wuxi and India series using LR, K-NN, and ANN

990 with PCA2

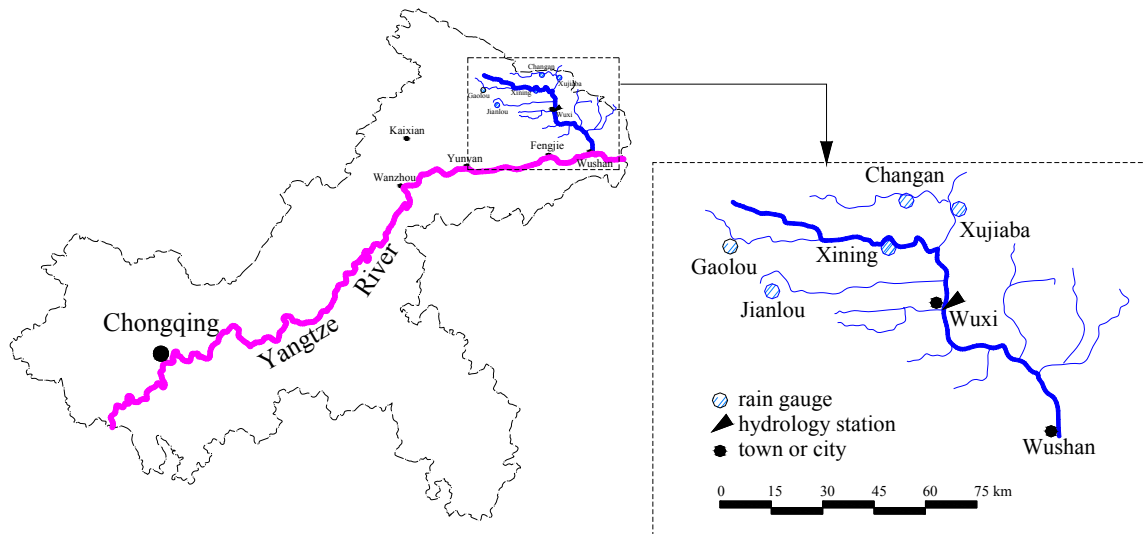
991 Table 8. Optimal  $p$  RCs for model inputs at various forecasting horizons

992 Table 9. Model performances at three forecasting horizons using MANN and ANN with the

993 SSA2

994 Table 10. RMSE of the LR model coupled with SSA2 using various  $L$

995



996

997

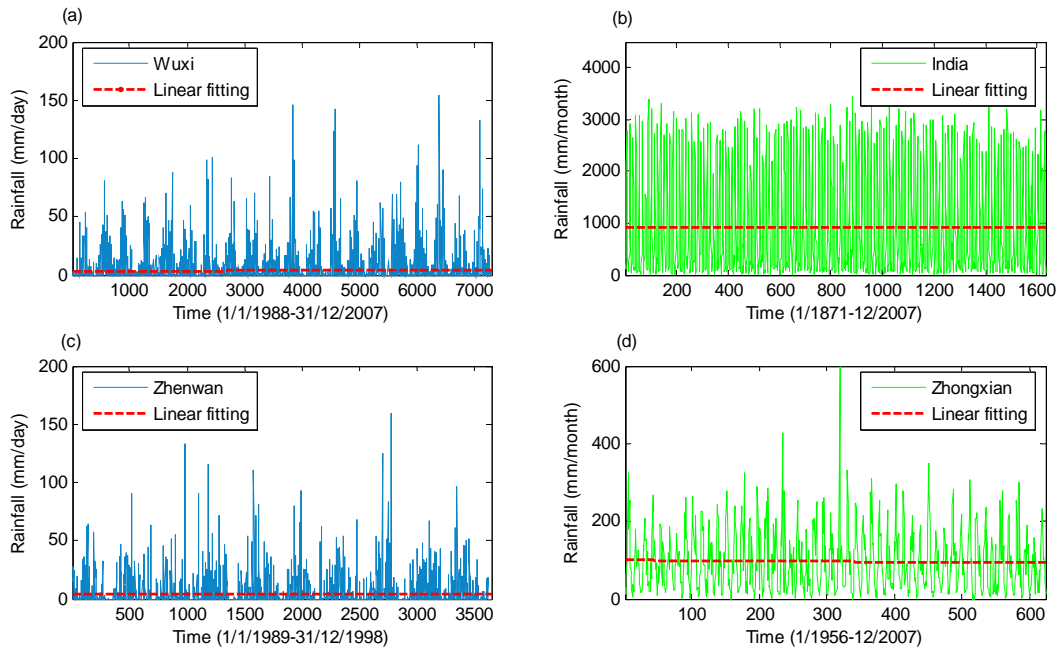
998

Figure 1.



999

1000

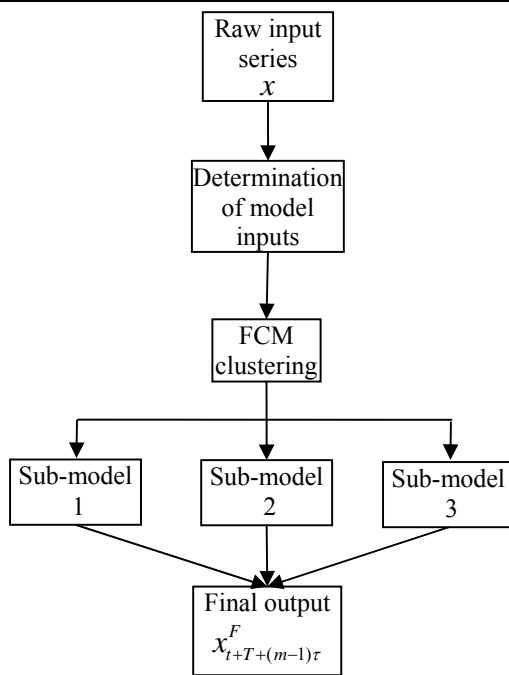


1001

1002

1003

Figure 2.



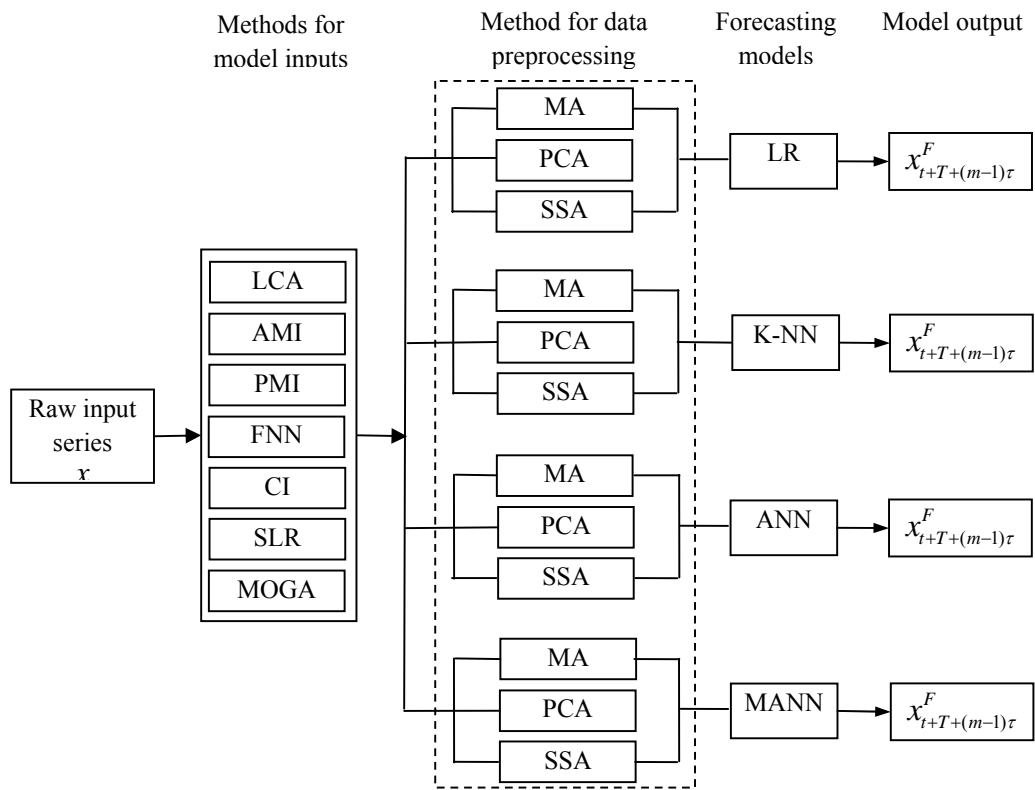
1004

1005

1006

Figure 3.

1007



1008

1009

Figure 4.

1010

1011

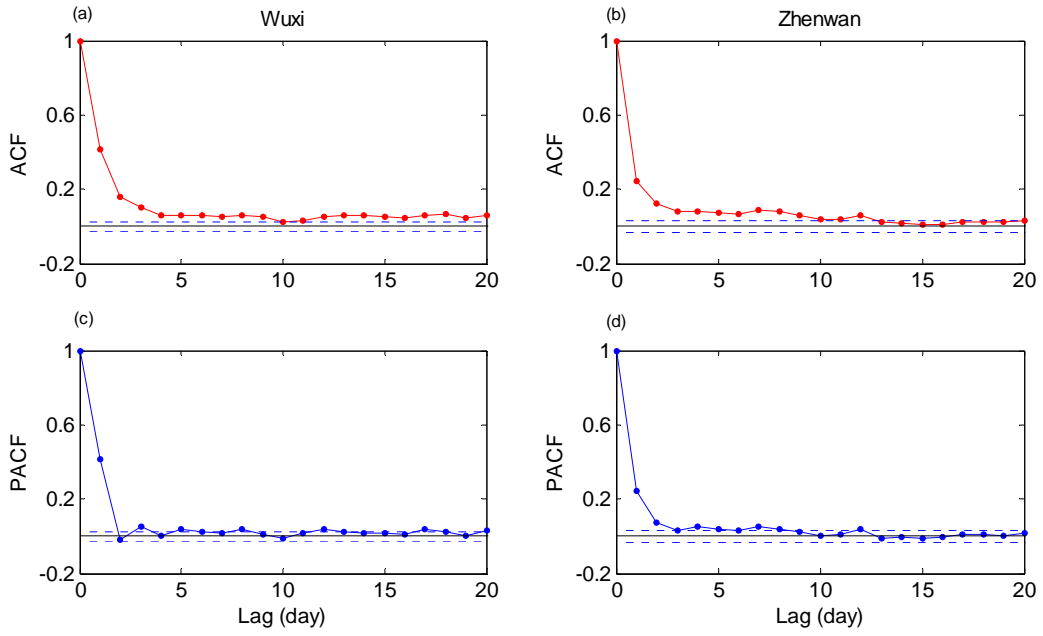


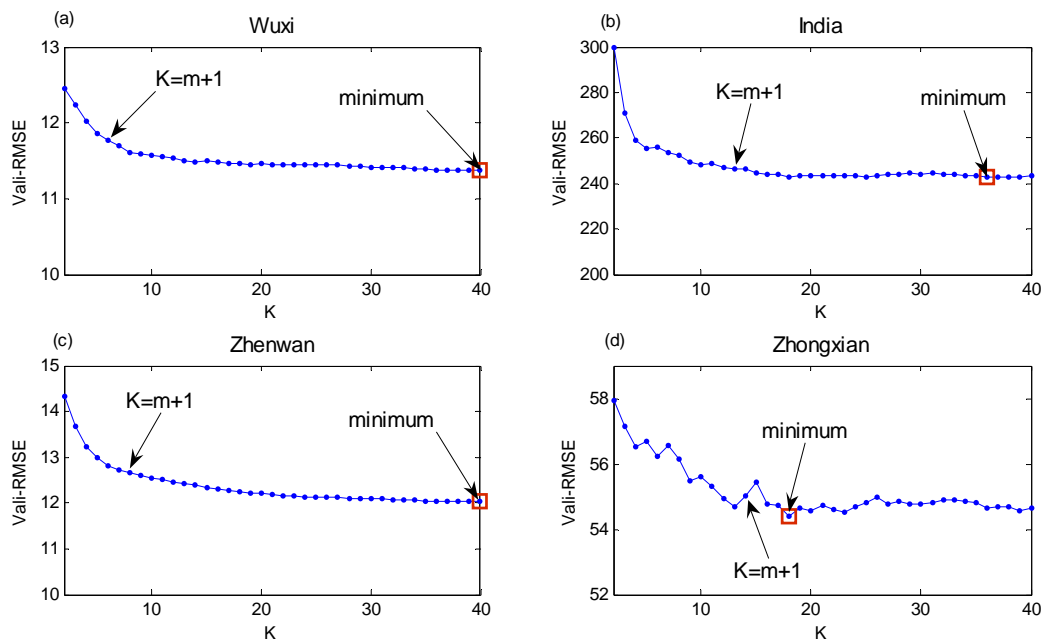
Figure 5.

1012

1013

1014

1015

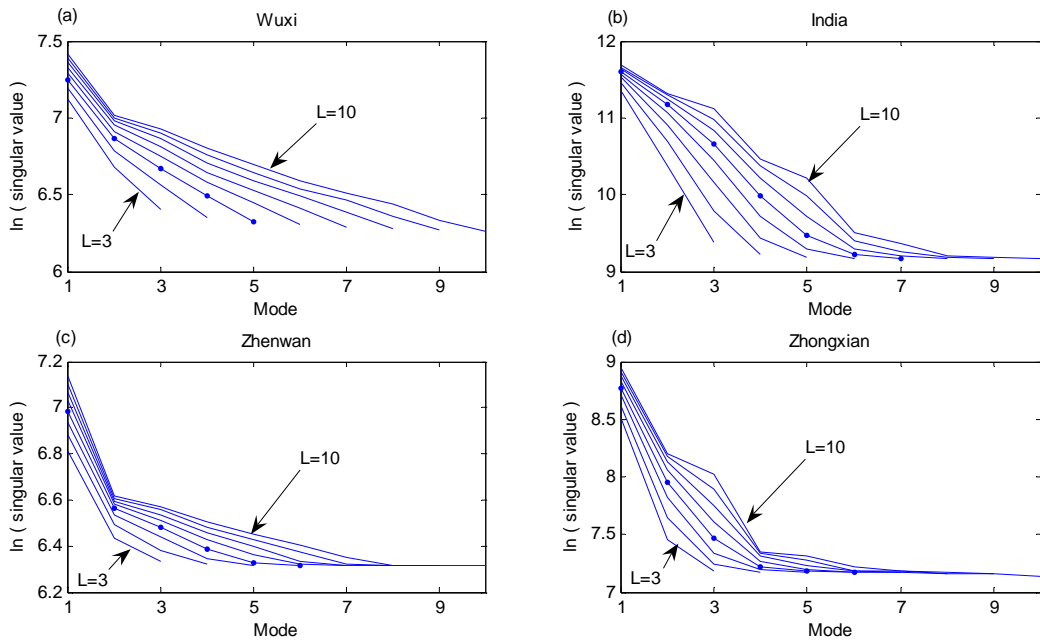


1016

1017

1018

Figure 6.



1019

1020

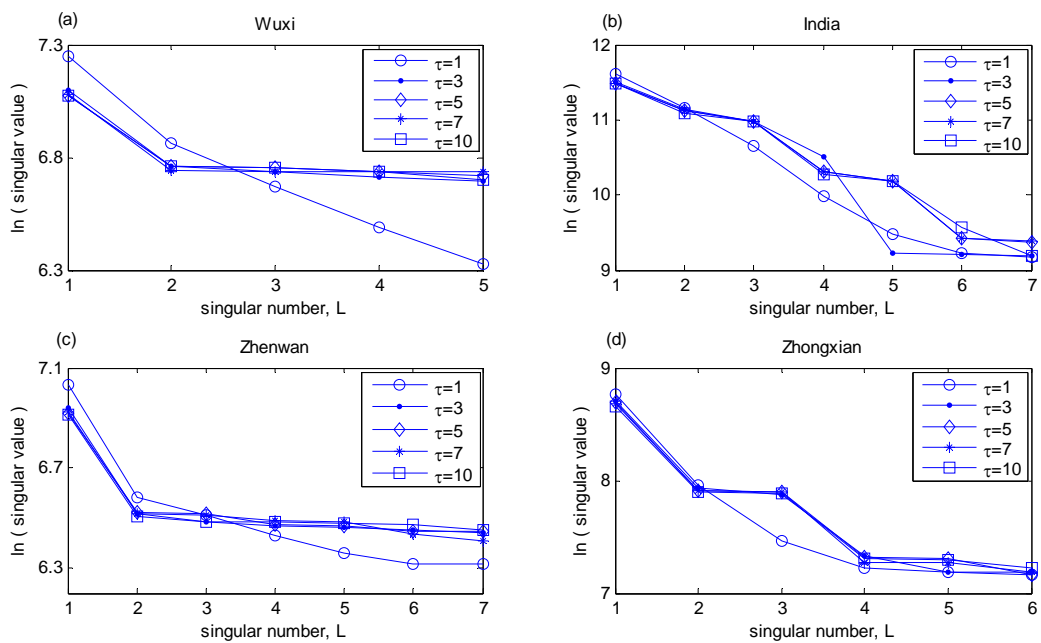
1021

Figure 7.

1022

1023

1024

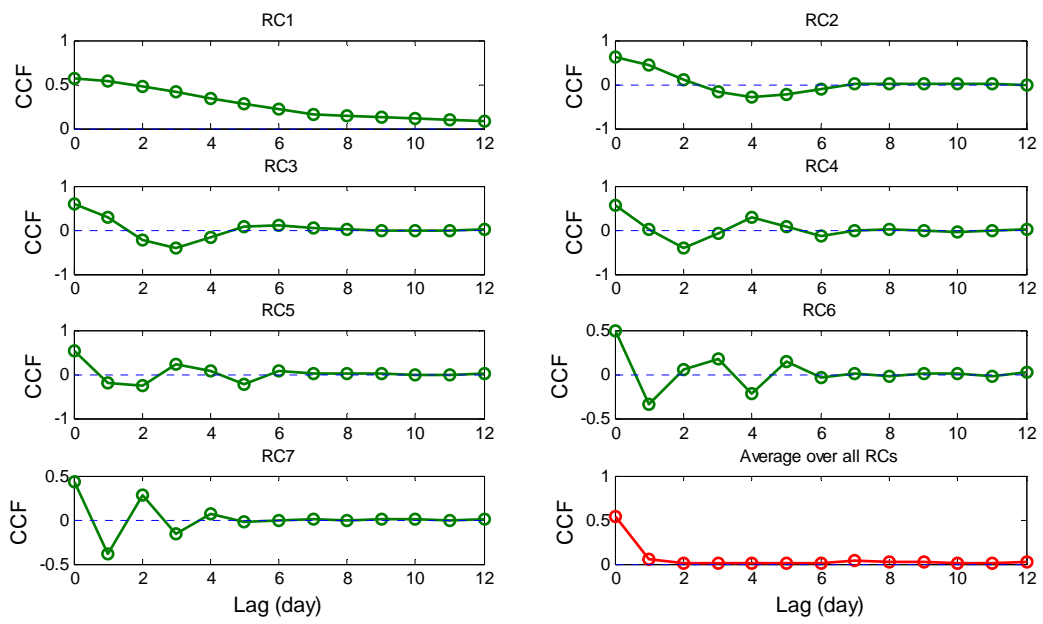


1025

1026

Figure 8.

1027



1028

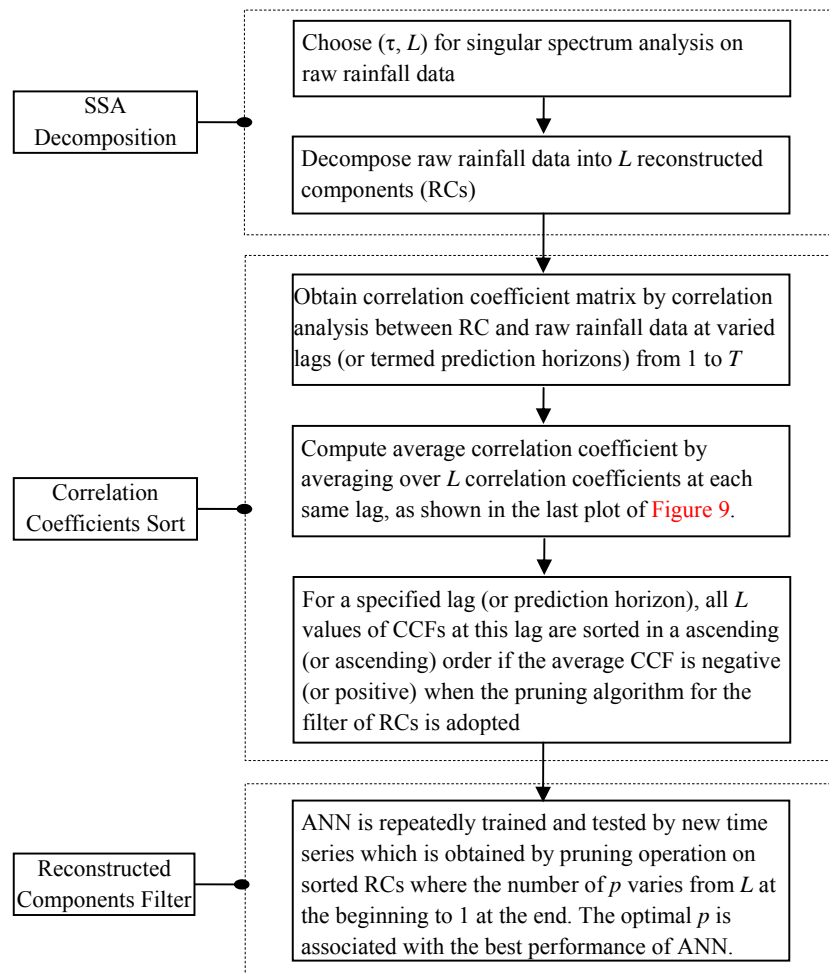
1029

1030

Figure 9.



1031



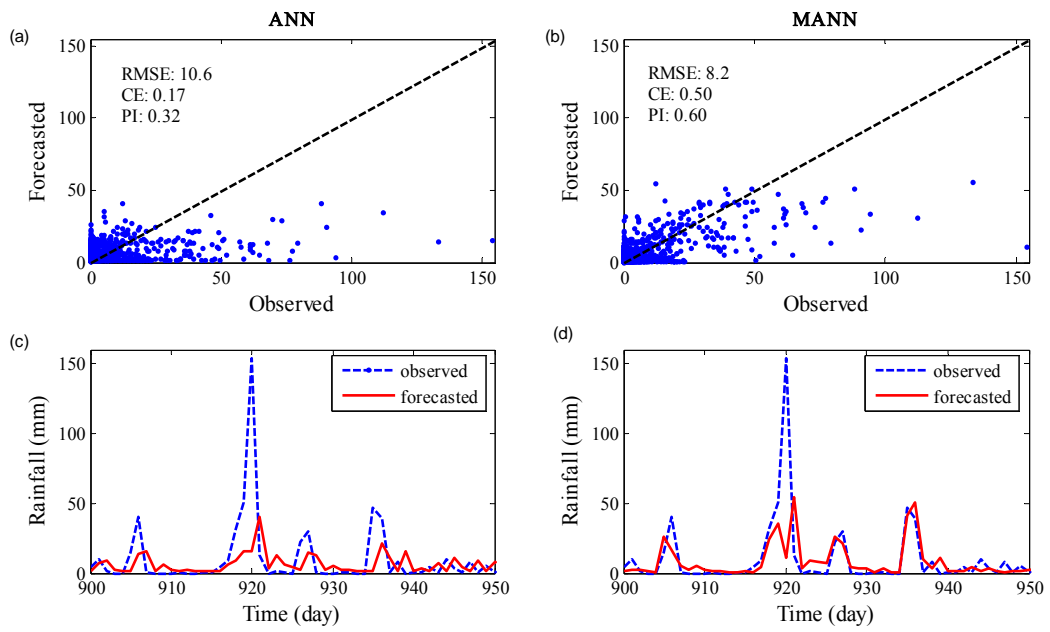
1032

1033

1034

Figure 10.

1035



1036

1037

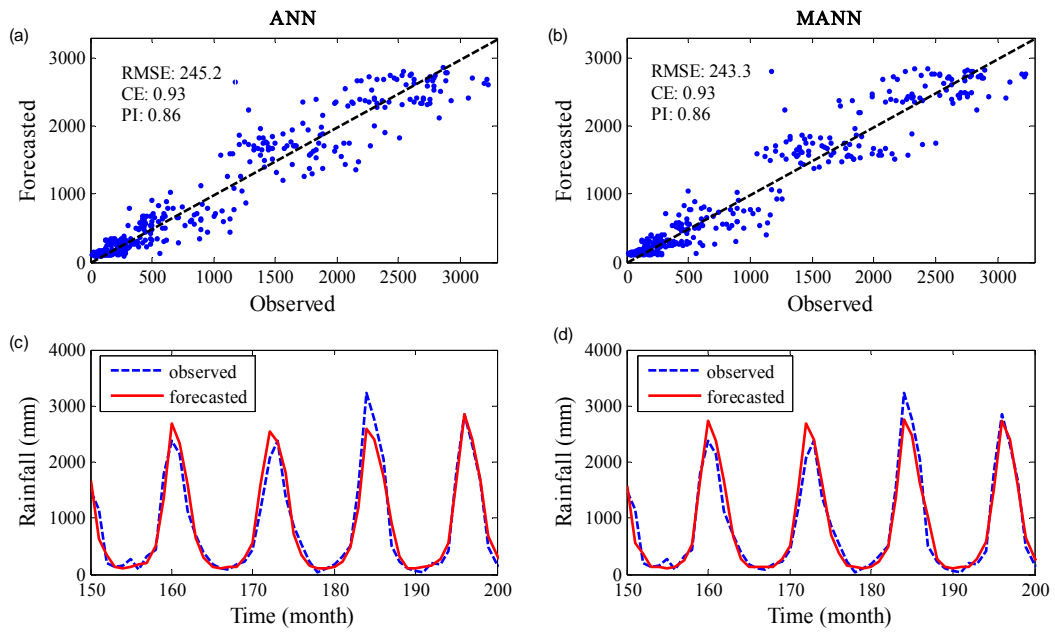
1038

Figure 11.

1039

1040

1041



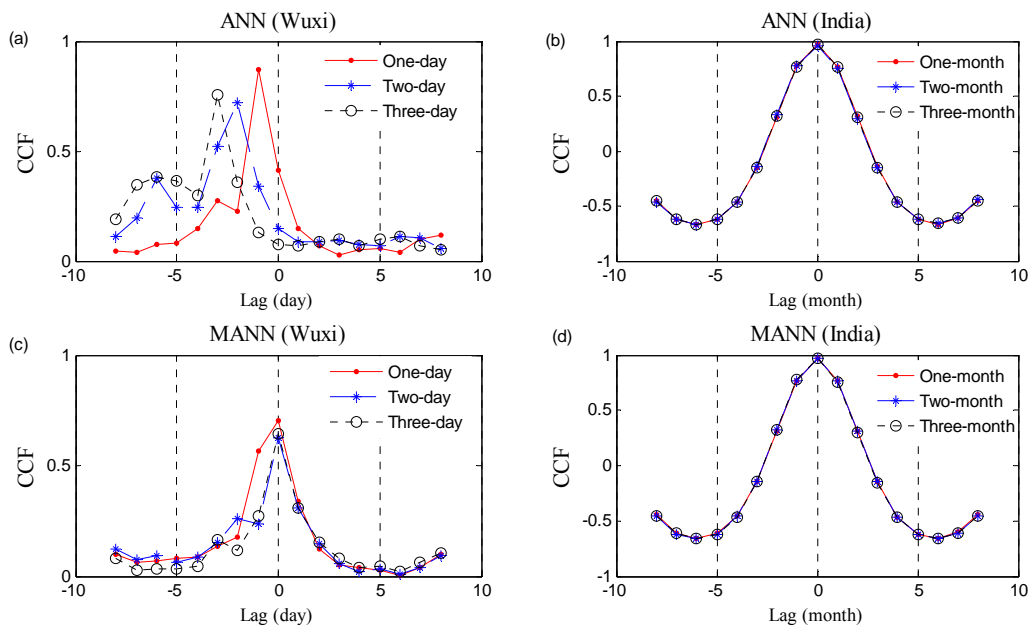
1042

1043

1044

Figure 12.

1045



1046

1047

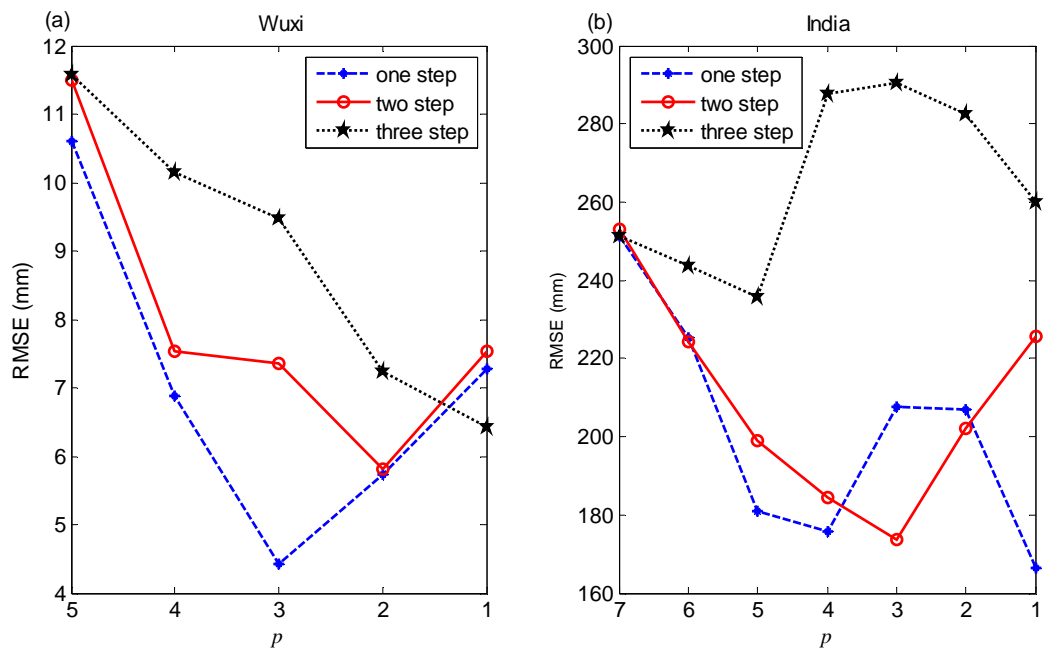
1048

Figure 13.

1049

1050

1051

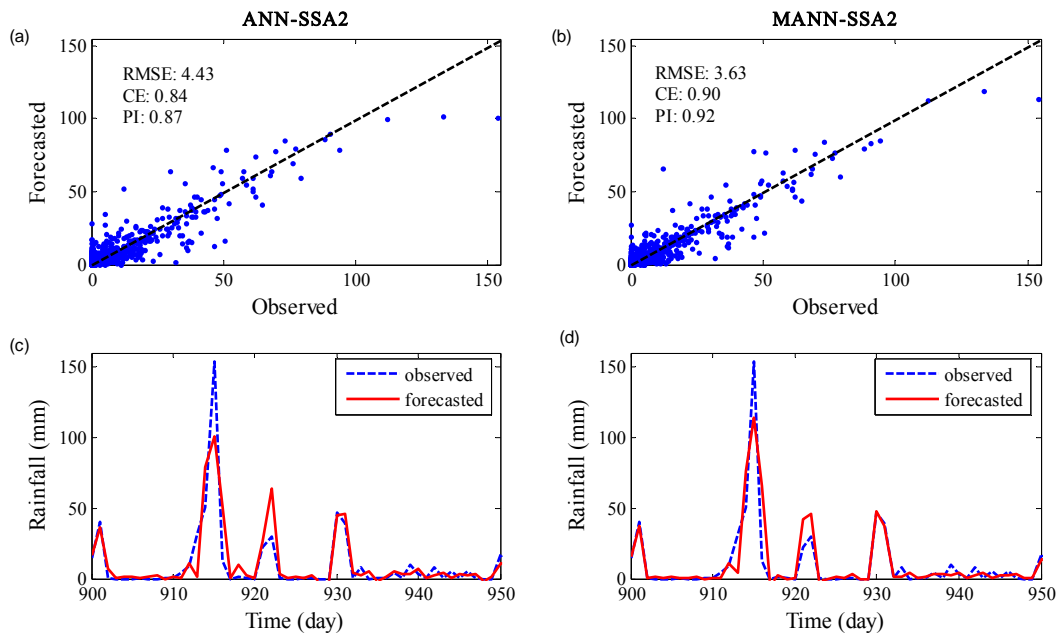


1052

1053

1054

Figure 14.



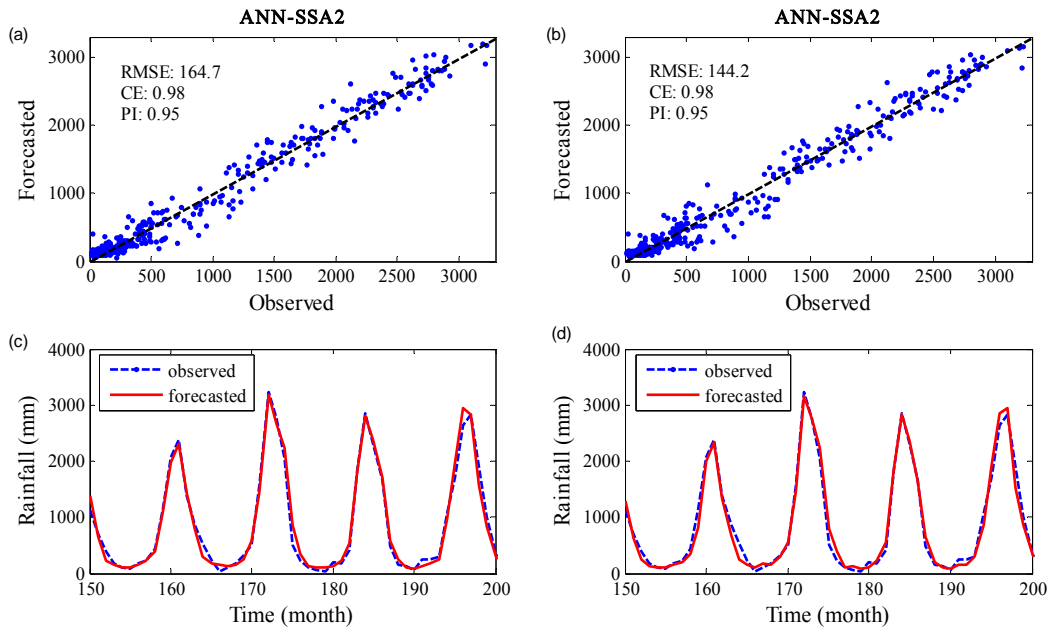
1055  
1056  
1057

Figure 15.

1058

1059

1060



1061

1062

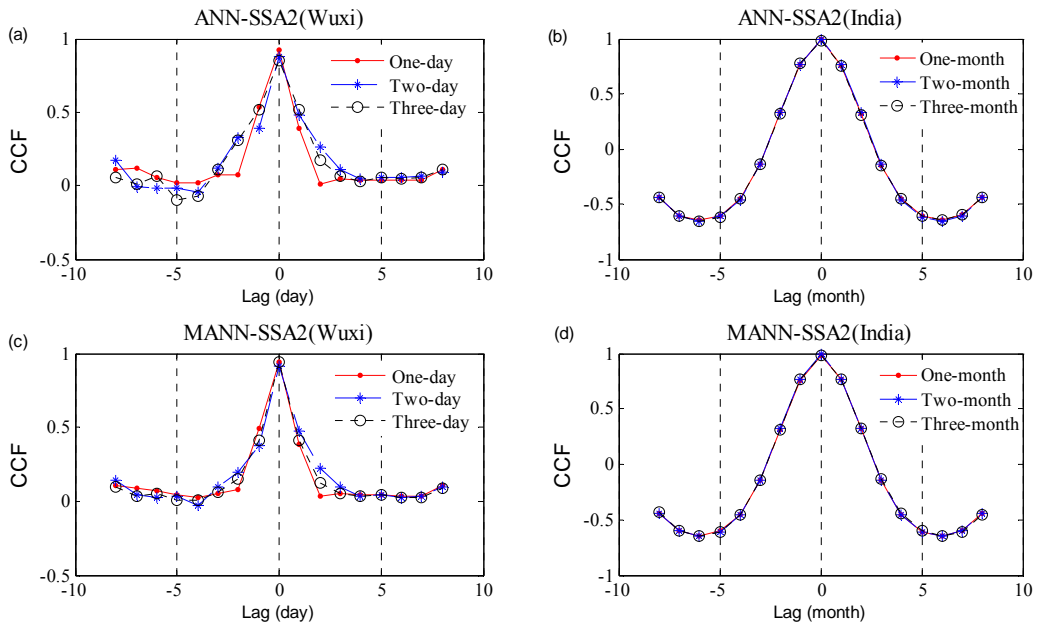
1063

Figure 16.

1064

1065

1066



1067

1068

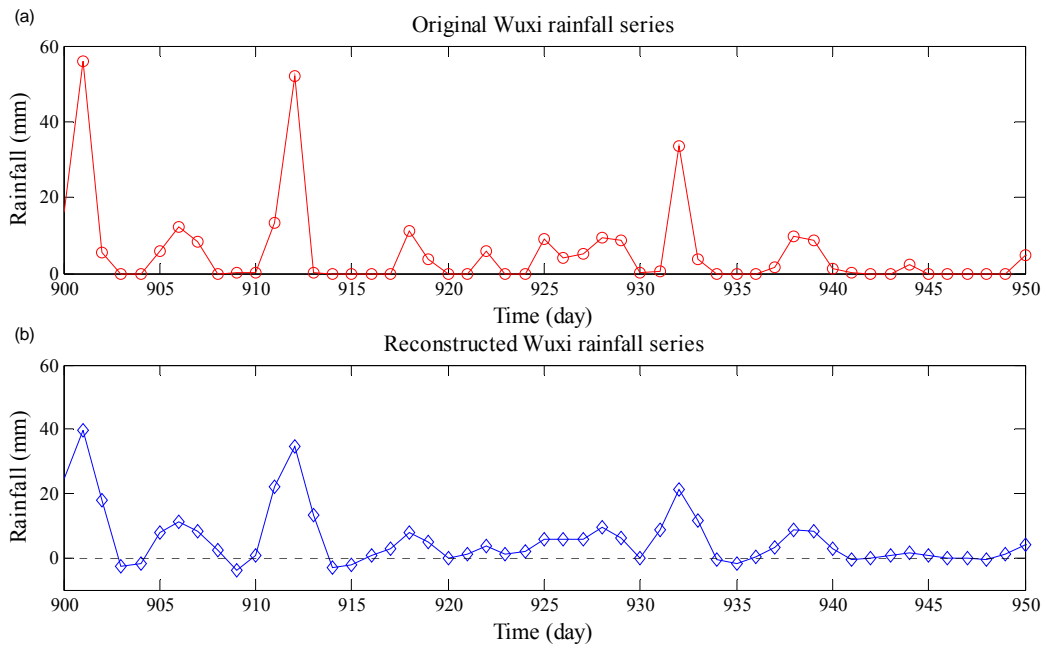
1069

Figure 17.



1070

1071



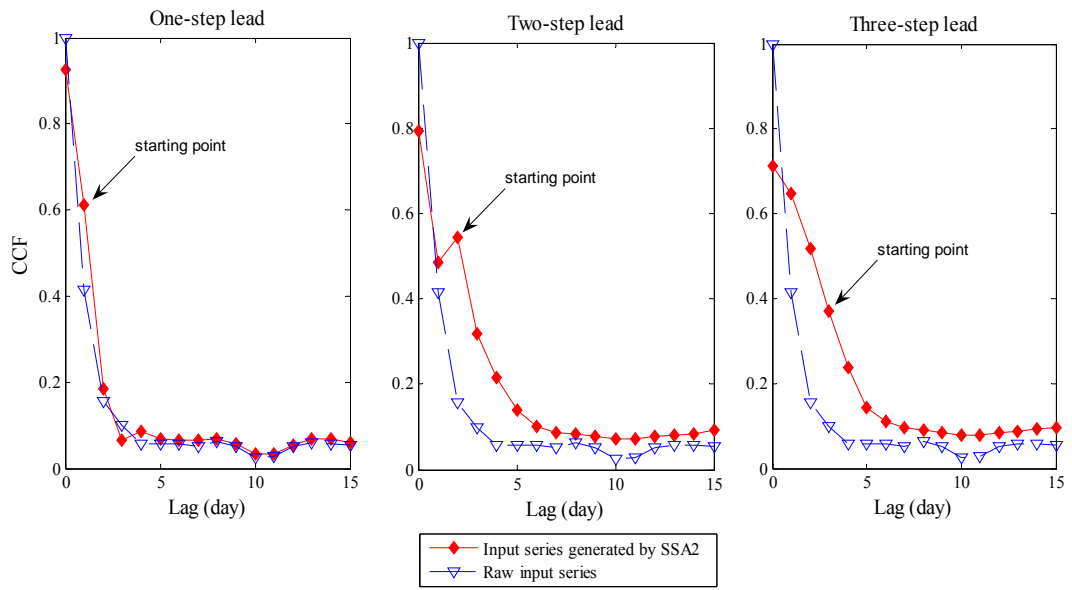
1072

1073

1074

Figure 18.

1075



1076

1077

1078

Figure 19.

1079

**Table 11.** Pertinent information for four watersheds and the rainfall data

Watershed and datasets	Statistical parameters						Watershed area and data period
	$\mu$ (mm)	$S_x$ (mm)	$C_v$	$C_s$	$X_{\min}$ (mm)	$X_{\max}$ (mm)	
<b>Wuxi</b>							
Original data	3.67	10.15	0.36	5.68	0.00	154	Area:
Training	3.81	10.94	0.35	6.27	0.00	147	2 000 km <sup>2</sup>
Cross-validation	3.42	8.87	0.39	4.96	0.00	102	Data period:
Testing	4.03	11.60	0.35	5.46	0.00	154	Jan., 1988- Dec., 2007
<b>Zhenwan</b>							
Original data	4.3	11.0	0.39	4.94	0.0	159	Area:
Training	4.3	11.2	0.38	5.60	0.0	159	7554 km <sup>2</sup>
Cross-validation	4.7	11.2	0.42	4.22	0.0	125	Data period:
Testing	4.0	10.9	0.37	4.97	0.0	133	Jan., 1989- Dec., 1998
<b>India</b>							
Original data	906.7	951.6	1.0	0.9	3.0	3460	Area:
Training	904.8	955.7	0.9	0.9	3.0	3393	all India
Cross-validation	918.2	969.5	0.9	1.0	8.0	3460	Data period:
Testing	898.9	927.4	1.0	0.9	16.0	3232	Jan., 1871- Dec., 2007
<b>Zhongxian</b>							
Original data	96.2	79.2	1.2	1.2	0.0	599	Area:
Training	97.2	77.5	1.3	0.9	0.0	429	
Cross-validation	98.6	86.8	1.1	1.9	0.0	599	Data period:
Testing	91.8	74.9	1.2	0.8	0.0	306	Jan., 1956- Dec., 2007

1080

1081

1082

**Table 12.** Comparison of methods to determine mode inputs using ANN model

Watershed	Methods	$\tau$	$m$	Effective inputs <sup>a</sup>	Identified ANN	RMSE
<b>Wuxi</b>						
	LCA	1	20	The last 5	(5-5-1)	10.74
	AMI	1	12	Except for Xt-10,t-9	(10-3-1)	10.91
	PMI <sup>b</sup>	1	12	Xt,t-1,t-3,t-5,t-7,t-10,t-4	(7-8-1)	10.85
	FNN	1	20	The last 14	(14-3-1)	11.02
	CI	4	20	Nil		
	SLR	1	12	Xt-11,t-7,t-4,t-2,t-1,t	(6-3-1)	10.94
	MOGA	1	12	Xt, t-1	(2-6-1)	10.55
<b>Zhenwan</b>						
	LCA	1	20	The last 7	(7-4-1)	11.03
	AMI	1	12	Except for Xt-11,t-10,t-9,t-8,t-2	(7-5-1)	10.95
	PMI	1	12	Xt-4,t,t-1,t-3,t-11,t-5,t-10,t-6,t-9	(10-4-1)	10.98
	FNN	1	20	Last 14	(14-3-1)	11.08
	CI	3	20	Nil		
	SLR	1	12	Xt-11,t-7,t-6,t-3,t-1,t	(6-3-1)	11.01
	MOGA	1	12	Xt,t-4,t-7,t-9,t-11	(5-8-1)	10.43
<b>India</b>						
	LCA	1	20	the last 12	(12-5-1)	256.22
	AMI	1	12	the last 12	(12-5-1)	256.22
	PMI	1	12	Xt-11,t-10,t-5,t	(4-5-1)	275.06
	FNN	1	20	the last 5	(5-9-1)	286.04
	CI	4	20	nil		
	SLR	1	12	except for Xt-4	(11-9-1)	258.13
	MOGA	1	12	Xt-11,t-9,t-7,t-5,t-4,t-1,t	(7-1-1)	277.57
<b>Zhongxian</b>						
	LCA	1	20	the last 13	(13-3-1)	51.70
	AMI	1	12	Xt-11,t-10,t-6,t-5,t-4,t	(6-5-1)	54.67
	PMI	1	12	Xt-11,t,t-9,t-7,t-7	(5-9-1)	55.39
	FNN	1	20	the last 4	(4-7-1)	59.78
	CI	3	20	nil		
	SLR	1	12	Xt-11,t-7,t-6,t-5,t-3,t	(6-6-1)	55.47
	MOGA	1	12	Xt-11,t-10,t-6,t-3,t	(5-2-1)	53.93

1083

1084

1085

Note:<sup>a</sup> for the convenience of writing down effective inputs, “Xt, t-1” stands for Xt, Xt-1; <sup>b</sup> effective inputs from PMI are in descending order of priority.

1086

**Table 13.** Performance comparison of ANN with different data-transformed methods

Watershed	Data Transformation	RMSE			CE		
		1	2	3 <sup>a</sup>	1	2	3
<b>Wuxi</b>							
	Std_raw	10.77	11.54	11.62 <sup>b</sup>	0.14	0.01	0.00
	Norm_raw	10.57	11.49	11.59	0.17	0.02	0.00
	Std_nth_root	11.00	12.02	12.10	0.10	-0.07	-0.09
	Norm_nth_root	11.15	12.01	12.09	0.08	-0.07	-0.09
<b>Zhenwan</b>							
	Std_raw	11.03	11.11	11.16	0.03	0.02	0.01
	Norm_raw	10.72	11.06	11.14	0.09	0.03	0.02
	Std_nth_root	11.25	11.68	11.75	-0.01	-0.09	-0.10
	Norm_nth_root	11.34	11.70	11.74	-0.02	-0.09	-0.09
<b>Wuxi</b>							
	Std_raw	256.22	250.51	249.46	0.92	0.93	0.93
	Norm_raw	251.74	246.48	250.99	0.93	0.93	0.93
	Std_nth_root	259.81	253.42	256.43	0.92	0.93	0.92
	Norm_nth_root	252.75	251.95	259.00	0.93	0.93	0.92
<b>Zhongxian</b>							
	Std_raw	54.26	54.23	53.91	0.48	0.48	0.48
	Norm_raw	52.91	53.10	52.78	0.50	0.50	0.51
	Std_nth_root	52.15	53.44	53.17	0.52	0.49	0.50
	Norm_nth_root	52.27	53.37	54.30	0.51	0.49	0.48

<sup>a</sup> Numbers of "1, 2, and 3" denote one-, two-, and three-day-ahead forecasting;

<sup>b</sup> Result is average over 10 best runs from total 20 runs;

1087  
1088  
1089

1090

**Table 14.** Model performances at three forecasting horizons under the normal mode

Watershed Model	RMSE			CE			PI		
	1*	2*	3*	1	2	3	1	2	3
<b>WuXi</b>									
Naïve	12.2	16.0	16.5	0.05	-0.61	-0.72	0.00	0.00	0.00
LR	10.9	11.9	12.0	0.12	-0.05	-0.07	0.28	0.41	0.43
K-NN	11.8	12.4	12.6	-0.03	-0.14	-0.18	0.16	0.36	0.38
ANN	10.6	11.5	11.6	0.17	0.02	0.00	0.32	0.45	0.47
MANN	8.2	9.2	9.0	0.50	0.38	0.40	0.60	0.65	0.68
<b>Zhenwan</b>									
Naïve	12.4	12.2	13.6	-0.53	-0.49	-0.84	0.00	0.00	0.00
LR	11.1	11.3	11.4	0.02	-0.02	-0.03	0.39	0.42	0.45
K-NN	12.7	12.7	12.8	-0.27	-0.28	-0.30	0.21	0.28	0.31
ANN	10.7	11.1	11.1	0.09	0.03	0.02	0.43	0.45	0.48
MANN	7.9	9.6	9.9	0.50	0.27	0.23	0.69	0.59	0.59
<b>India</b>									
Naïve	643.1	1084.5	1399.2	0.52	-0.37	-1.28	0.00	0.00	0.00
LR	286.8	301.6	302.7	0.90	0.89	0.89	0.80	0.92	0.95
K-NN	246.6	257.3	251.2	0.93	0.92	0.93	0.85	0.94	0.97
ANN	245.2	245.9	247.2	0.93	0.93	0.93	0.86	0.95	0.97
MANN	243.3	241.8	244.4	0.93	0.93	0.93	0.86	0.95	0.97
<b>Zhongxian</b>									
Naïve	75.7	91.9	109.2	-0.03	-0.51	-1.13	0.00	0.00	-0.02
LR	56.1	57.7	58.4	0.44	0.41	0.39	0.46	0.60	0.71
K-NN	55.0	56.0	57.2	0.46	0.44	0.42	0.48	0.63	0.72
ANN	52.5	54.4	54.3	0.51	0.48	0.48	0.52	0.65	0.75
MANN	50.3	50.2	53.2	0.55	0.55	0.50	0.56	0.70	0.76

\* The number of "1, 2, and 3" denote one-, two-, and three-step-ahead forecasts

1091

1092

1093

1094

**Table 15.** Model performances of ANN-MA using the Wuxi data

Prediction horizons	Performance index	Window length (k) for MA									
		1	2	3	4	5	6	7	8	9	10
One-step											
	RMSE	10.60	10.70	10.63	10.72	10.77	10.70	10.83	10.83	10.72	10.68
	CE	0.17	0.15	0.16	0.15	0.14	0.15	0.13	0.13	0.15	0.15
	PI	0.32	0.31	0.32	0.31	0.30	0.31	0.29	0.29	0.31	0.31
Two-step											
	RMSE	11.50	11.51	11.51	11.50	11.53	11.56	11.55	11.47	11.45	11.45
	CE	0.02	0.02	0.02	0.02	0.01	0.01	0.01	0.02	0.03	0.03
	PI	0.45	0.44	0.44	0.45	0.44	0.44	0.44	0.45	0.45	0.45
Three-step											
	RMSE	11.60	11.58	11.58	11.55	11.61	11.58	11.56	11.51	11.52	11.52
	CE	0.00	0.00	0.00	0.01	0.00	0.00	0.01	0.02	0.01	0.01
	PI	0.47	0.47	0.47	0.48	0.47	0.47	0.48	0.48	0.48	0.48

1095

1096

**Table 6.** Multiple-step predictions for Wuxi and India series using LR, K-NN, and ANN

1097

with PCA1

Watershed	Performance index	V (%) <sup>1</sup>	LR			K-NN			ANN		
			1*	2*	3*	1	2	3	1	2	3
<b>Wuxi</b>											
RMSE	85	85	11.0	11.9	12.0	12.1	12.5	12.7	10.6	11.5	11.6
	90	85	11.0	11.9	12.0	12.1	12.5	12.7	10.7	11.5	11.6
	95	85	10.9	11.9	12.0	11.8	12.4	12.6	10.6	11.5	11.6
	100	85	10.9	11.9	12.0	11.8	12.4	12.6	10.6	11.5	11.6
CE	85	85	0.12	-0.05	-0.07	-0.04	-0.15	-0.19	0.16	0.01	0.00
	90	85	0.12	-0.05	-0.07	-0.04	-0.15	-0.19	0.16	0.02	0.00
	95	85	0.12	-0.05	-0.07	-0.03	-0.14	-0.18	0.16	0.02	0.00
	100	85	0.12	-0.05	-0.07	-0.03	-0.14	-0.18	0.17	0.02	0.00
PI	85	85	0.27	0.41	0.43	0.12	0.34	0.36	0.32	0.44	0.47
	90	85	0.27	0.41	0.43	0.12	0.34	0.36	0.31	0.45	0.47
	95	85	0.28	0.41	0.43	0.16	0.36	0.38	0.32	0.45	0.47
	100	85	0.28	0.41	0.43	0.16	0.36	0.38	0.32	0.45	0.47
<b>India</b>											
RMSE	85	85	410.9	320.6	457.7	275.9	262.7	281.1	250.4	256.1	247.0
	90	85	294.9	307.8	311.1	260.3	256.2	276.8	248.1	252.3	249.0
	95	85	291.6	305.0	304.6	255.3	256.5	265.0	247.7	254.2	251.4
	100	85	286.8	301.6	302.7	246.6	257.3	251.2	245.2	245.9	247.2
CE	85	85	0.81	0.89	0.78	0.91	0.91	0.90	0.93	0.92	0.93
	90	85	0.90	0.89	0.89	0.92	0.91	0.91	0.93	0.93	0.93
	95	85	0.90	0.89	0.89	0.92	0.91	0.91	0.93	0.92	0.93
	100	85	0.90	0.89	0.89	0.93	0.92	0.93	0.92	0.92	0.93
PI	85	85	0.61	0.92	0.90	0.81	0.93	0.96	0.85	0.94	0.97
	90	85	0.79	0.92	0.95	0.83	0.94	0.96	0.85	0.95	0.97
	95	85	0.80	0.92	0.95	0.84	0.94	0.96	0.85	0.95	0.97
	100	85	0.80	0.92	0.95	0.85	0.94	0.97	0.84	0.94	0.97

1098

Note: \* "1, 2, and 3" denote one-, two-, and three-step-ahead forecasts; <sup>1</sup> "V" stands for the percentage of total variance.

1099

1100



1101 **Table 16.** Multiple-step predictions for Wuxi and India series using LR, K-NN, and  
 1102 ANN with PCA2

Watershed	Performance index	V (%) <sup>1</sup>	LR			K-NN			ANN		
			1*	2*	3*	1	2	3	1	2	3
<b>Wuxi</b>											
RMSE	85	85	10.8	11.6	11.6	11.5	12.2	12.7	10.6	11.5	11.6
	90	85	10.8	11.6	11.6	11.5	12.2	12.7	10.6	11.5	11.6
	95	85	10.9	11.9	12.0	11.8	12.4	12.6	10.6	11.5	11.6
	100	85	10.9	11.9	12.0	11.8	12.4	12.6	10.6	11.5	11.6
CE	85	85	0.14	0.01	0.00	0.02	-0.11	-0.19	0.16	0.02	0.00
	90	85	0.14	0.01	0.00	0.02	-0.11	-0.19	0.16	0.02	0.00
	95	85	0.12	-0.05	-0.07	-0.03	-0.14	-0.18	0.17	0.02	0.00
	100	85	0.12	-0.05	-0.07	-0.03	-0.14	-0.18	0.16	0.02	0.00
PI	85	85	0.30	0.44	0.47	0.20	0.37	0.37	0.32	0.44	0.47
	90	85	0.30	0.44	0.47	0.20	0.37	0.37	0.32	0.45	0.47
	95	85	0.28	0.41	0.43	0.16	0.36	0.38	0.32	0.45	0.47
	100	85	0.28	0.41	0.43	0.16	0.36	0.38	0.32	0.45	0.47
<b>India</b>											
RMSE	85	85	482.9	413.0	800.6	254.7	248.9	253.1	241.7	247.2	249.8
	90	85	352.8	357.8	600.6	253.1	249.4	250.4	245.0	247.9	247.8
	95	85	326.5	331.9	376.1	247.8	246.1	246.1	243.5	249.0	244.8
	100	85	286.8	301.6	302.7	246.6	257.3	251.2	247.6	252.3	247.1
CE	85	85	0.73	0.80	-2.74	0.92	0.93	0.93	0.93	0.93	0.93
	90	85	0.86	0.85	0.58	0.93	0.93	0.93	0.93	0.93	0.93
	95	85	0.88	0.87	0.84	0.93	0.93	0.93	0.93	0.93	0.93
	100	85	0.90	0.89	0.89	0.93	0.92	0.93	0.93	0.93	0.93
PI	85	85	0.44	0.86	-1.75	0.84	0.95	0.97	0.86	0.95	0.97
	90	85	0.70	0.89	0.81	0.85	0.95	0.97	0.86	0.95	0.97
	95	85	0.74	0.91	0.93	0.85	0.95	0.97	0.86	0.95	0.97
	100	85	0.80	0.92	0.95	0.85	0.94	0.97	0.85	0.95	0.97

1103

1104

1105

**Table 17.** Optimal  $p$  RCs for model inputs at various forecasting horizons

Watershed Model	Prediction horizons	Supervised filter (SSA1)		Unsupervised filter (SSA2)	
		Optimal $p$ RCs	RMSE	Optimal $p$ RCs	RMSE
<b>Wuxi</b>					
LR	1	1* 2*	6.01	1 2	6.01
	2	1 5	7.73	1 5	7.73
	3	1	8.40	1	8.40
K-NN	1	1	8.02	2 3	7.17
	2	1	8.41	2 4	8.03
	3	1	9.99	2	9.69
ANN	1	1 2 3	4.43	1 2 3	4.43
	2	1 5	5.82	1 5	5.57
	3	1	6.42	1	6.25
<b>Zhenwan</b>					
LR	1	1 2 3	7.19	1 2 3	7.19
	2	1 7 2	7.99	1 2 7	7.99
	3	1 5	8.81	1 5	8.81
K-NN	1	1 2 3 4 5	9.84	3 6	7.64
	2	1	9.72	3 6	8.95
	3	1	10.33	2 5	10.24
ANN	1	1 2 3 4	5.55	5 6 7	5.02
	2	1 7 2	5.84	3 7	5.51
	3	1 5	6.58	3 7	5.56
<b>India</b>					
LR	1	2 1 3 4	185.95	1 2 3 4	185.95
	2	1 2	237.85	1 2	237.85
	3	3 4 2 7 1	299.14	1 2 6	287.16
K-NN	1	2 1 3 4 5	236.90	1 2 5 6	236.39
	2	1 2	247.44	1 2 5	242.65
	3	3 4 2 7	249.43	1 2 5 6	243.86
ANN	1	2	166.58	1 7	164.70
	2	1 2 7	173.57	1 2 7	166.30
	3	3 4 2 7 1	235.59	1 5 7	172.56
<b>Zhongxian</b>					
LR	1	1 2	40.06	1 2	40.06
	2	1 2 6	41.87	1 6	39.44
	3	3 6 2 4 1	58.29	1 5	41.53
K-NN	1	1 2	51.78	1 2	51.78
	2	1 2	53.86	1 2 3	53.32
	3	3 6 2	54.15	2 3	53.16
ANN	1	1 2 3	38.39	1 5 6	34.09
	2	1	44.49	1 5 6	39.45
	3	3 6	46.14	1 5	34.94

1106  
1107  
1108

Note: \* the numbers of "1, 2" stand for RC1 and RC2, and these numbers in the SSA1 column is in a descending order of CCFs shown in Figure 6.12.

1109 **Table 18.** Model performances at three forecasting horizons using MANN and ANN with the

1110

SSA2

Watershed Model	RMSE			CE			PI		
	1	2	3	1	2	3	1	2	3
<b>WuXi</b>									
ANN	4.43	5.57	6.25	0.84	0.78	0.70	0.87	0.88	0.84
MANN	3.63	4.32	3.93	0.90	0.86	0.89	0.92	0.92	0.94
<b>Zhenwan</b>									
ANN	5.02	5.51	5.56	0.81	0.75	0.71	0.88	0.85	0.84
MANN	3.18	3.20	3.31	0.92	0.92	0.91	0.95	0.95	0.95
<b>India</b>									
ANN	164.7	166.3	172.6	0.97	0.97	0.97	0.95	0.98	0.99
MANN	144.2	145.1	157.4	0.98	0.98	0.97	0.95	0.98	0.99
<b>Zhongxian</b>									
ANN	34.09	39.45	34.94	0.84	0.71	0.83	0.84	0.80	0.92
MANN	28.58	32.24	32.69	0.86	0.82	0.82	0.86	0.88	0.91

1111

1112

1113

1114

**Table 19.** RMSE of the LR model coupled with SSA2 using various  $L$

Watershed	Prediction horizons	$L$ in SSA							
		3	4	5	6	7	8	9	10
Wuxi	1	6.13	5.94	<b>6.01</b>	6.41	5.83	5.81	5.61	5.51
	2	7.79	7.62	<b>7.73</b>	8.14	7.71	7.75	7.62	7.66
	3	11.76	8.61	<b>8.40</b>	9.04	9.23	8.72	8.56	8.62
Zhenwan	1	7.74	7.49	7.31	7.29	<b>7.19</b>	6.99	7.08	6.84
	2	10.27	8.42	9.04	8.19	<b>7.99</b>	7.67	7.43	7.61
	3	11.28	10.66	10.06	9.33	<b>8.81</b>	8.91	9.42	9.28

1115

1116